European Polymer Journal 236 (2025) 114147

Contents lists available at ScienceDirect

European Polymer Journal

journal homepage: www.elsevier.com/locate/europolj

Core-shell polymeric micelles based on the 2-(hydroxyimino)aldehyde group as self-contained nanoreactors to obtain single and clustered ultra-small silver nanoparticles

Giancarlo Masci [a,*], Francesca D'Acunzo [b,*], Stefano Casciardi [c], Angela Cirigliano [d], Alessandra Del Giudice [a], Francesco Mura [e], Elena Passarini [d], Emily Schifano [d], Gabriella Maria Pastore [a], Carlotta Petrianni [a], Patrizia Gentili [a,b]

[a] Department of Chemistry, Sapienza University of Rome, P.le A. Moro 5, 00185 Roma, Italy
[b] Institute for Biological Systems (ISB), CNR, Sezione Meccanismi di Reazione, c/o Department of Chemistry, Sapienza University of Rome, P.le A. Moro 5, 00185 Rome, Italy
[c] National Institute for Insurance Against Accidents at Work (INAIL Research), Department of Occupational and Environmental Medicine, Epidemiology and Hygiene, Rome, Italy
[d] Sapienza University of Rome, Dept. of Biology and Biotechnologies, P.le A. Moro 5, 00185 Rome, Italy
[e] Department of Basic and Applied Sciences for Engineering (SBAI), Sapienza University of Rome, Via Antonio Scarpa 14, 00161 Rome, Italy

ARTICLE INFO

Keywords:
Polymeric micelles
Silver nanoparticles
Clusters
Block copolymers
2-(hydroxyimino)aldehyde

ABSTRACT

Colloidal Silver NanoParticles (AgNPs) are routinely obtained from Ag^+ salts with chemical reductants in the presence of polymers or small molecules as capping agents to control their size and shape and enhance their stability. The use of amine-containing polymers, polyethers and polyols for AgNPs fabrication circumvents the need for added reductants, thus avoiding purification steps and enhancing process sustainability. However, high temperatures or irradiation may still be needed, and characterization of the resulting chemical species may be difficult. In this work, we incorporate Ag^+ into pre-formed micelles obtained through a pH-gradient method from two block copolymers pTEGMA-*b*-pHIABMA (TEGMA: tetra(ethylene glycol) methyl ether methacrylate, 75 units; HIABMA: 4-[(hydroxyimino)aldehyde]butyl methacrylate), 38 or 73 units) and a 37:37 random copolymer pOEGMA-*r*-pHIABMA (OEGMA having nine EG units). The micelles act as self-contained nanoreactors through the oxidation of aldehyde groups to carboxylates (^{1}H and ^{13}C NMR), to yield AgNPs with polymer-dependent characteristics. The core–shell micelles obtained with the two block copolymers afford ultra-small (2 nm diameter) spherical AgNPs clustered within the polymer nanoaggregates (DLS, TEM, SAXS). More numerous AgNPs are embedded within the polymer having more HIABMA units. The loose micelles obtained with the random copolymer, instead, affords single 10 nm AgNPs. The polymer-coated AgNPs exhibit Surface Plasmon Resonance ($\lambda = 418$ nm). No significant change in the UV–Vis spectra and DLS measurements was observed over a six-month period at room temperature. TEM micrographs show that the 2 nm clusters of AgNPs are stable over 20 months at 4 °C, with no evidence of coalescence, although partial solubilization of Ag^+ ions occurs over time. Given the different arrangement of the ultra-small AgNPs within the polymeric matrices of different architecture, the proposed nanoreactors may provide new tools in the fields of metamaterials and nanoarchitectonics. As for antimicrobial effects, a preliminary evaluation of the microbiological activity of the 2 nm clustered AgNPs shows bacteriostatic activity against *Staphylococcus aureus* (5 μg mL^{-1} Ag), and bactericidal activity (11 μg mL^{-1} Ag) against *Pseudomonas aeruginosa*, in concentration ranges that are comparable to previous literature on ultra-small AgNPs.

* Corresponding authors.
E-mail addresses: giancarlo.masci@uniroma1.it (G. Masci), francesca.dacunzo@cnr.it (F. D'Acunzo).

https://doi.org/10.1016/j.eurpolymj.2025.114147
Received 24 May 2025; Received in revised form 7 July 2025; Accepted 13 July 2025
Available online 16 July 2025

1. Introduction

Metal nanoparticles (NPs) elicit great interest in the research community in the most diverse fields, from catalysis to nanomedicine [1]. A well-known phenomenon associated with metal NPs is Surface Plasmon Resonance (SPR), a property exhibited in very different setups, from metal thin films, to colloidal NPs [2,3]. The relevance of colloidal plasmonics in nanoarchitectonics for biomedical applications is highlighted in a recent review article by Mejía-Salazar and Oliveira [4]. SPR originates from the coherent oscillation of free electrons in the very close conduction and valence bands upon excitation with a wavelength that depends on dielectric medium, chemical surroundings and, most importantly, particle size, shape and spatial arrangement [5,6]. Spherical silver nanoparticles (AgNPs) usually exhibit a band with a maximum spanning 410 – 500 nm as particle diameter increases from 5 to 100 nm [7]. However, for a given size, SPR spectra can be complex and red-shifted up to 800–1200 nm, depending on the shape of the AgNPs (e.g. cube, tetrahedron, thin disc etc [8].). AgNPs have been employed in the fabrication of nanocomposite materials for pollutants photodegradation [9] and metamaterials for the next generation of ultrathin optical components [10]. AgNPs can also be viewed as the modern version of ancient germicidal macroscale materials [11,12]. They find application as antimicrobial agents in very diverse fields, e.g. water treatment, agriculture, dentistry, wound healing, food packaging [1]. They are used for surface modification, with a particular emphasis on the prevention of infections on implants [13–15]. Furthermore, the emerging problem of multidrug resistance demands elucidation of their mechanism of action in connection with their size and shape [16–18]. Thanks to their high surface-to-volume ratio, AgNPs are very efficient at releasing Ag^+ ions, which interact with sulfidryl groups in cell membranes and with proteins and enzymes inside the cells, they cause an increase in reactive oxygen species (ROS), and tamper with DNA replication [19,20]. However, AgNPs should not be viewed as simple Ag^+ reservoirs, since particle-specific effects are also believed to come into play [21]. For instance, AgNPs may entail physical disruption of cell membranes, thus enhancing permeability of Ag^+ in a synergistic fashion [22]. All of these effects are size- and shape-dependent, with different microorganisms being more or less sensitive to AgNP size [23–25]. Depending on bacterial strain, Minimum Bactericidal Concentrations (MBCs) have been reported to increase by 3–5 times (from tens to hundreds μg mL^{-1}) upon increasing AgNP sizes from 5 to 100 nm [7]. It should also be noted that cytotoxicity parallels the enhanced antimicrobial activity of smaller AgNPs [26].

On these grounds, ongoing research on the fabrication of AgNPs focuses on controlling their size and shape, enhancing their stability in colloidal systems, and keeping the use of chemicals to a minimum [27]. In fact, AgNPs are routinely obtained from Ag^+ using chemical reductants such as sodium borohydride, hydrazine, ascorbic acid or sodium citrate. However, the use of added reductants entails purification steps, such as centrifugation, rinsing with ethanol, filtration or dialysis, thereby affecting the environmental and economical sustainability of the process. Synthesis of metal nanoparticles using plant extracts, which contain natural reductants of different types, is one of the most simple, convenient and environmentally friendly method to reduce the use of toxic chemicals [28]. With materials such as cellulose, citrus peel, chitosan, brown marine algae extract and many more, AgNPs of average size down to a few nm have been obtained, showing effective bactericidal activity [29]. However, surface modification (*capping*) of AgNPs with polymers of suitable composition and architecture can afford improved size control and colloidal stability, with a significant impact on shelf life, bactericidal activity, efficacy and safety in *in vivo* systems [3,16,30–32]. To this end, polymers such as PVP and polymethacrylates, are used in combination with chemical reductants to obtain AgNPs [33–35]. As an alternative, Ag^+ reduction is achieved thermally with PVA, Pluronics or other polyethers [36,37], or by generating PEO macroradicals by UV or even x-ray irradiation [38,39]. Amine-containing polymers and dendrimers have been proposed for the simultaneous production and stabilization of AgNPs without the need for reducing agents, high temperature or radiation [40,41]. Amine groups are believed to act as reductants towards noble metals cations through a one-electron process [42]. The fate of the resulting amine radical cations has been investigated in the most diverse fields, from electrochemistry to enzymatic reaction mechanisms. It depends on the nature of the amine [43] and it ranges from polymerization to dealkylation with release of carbonyl compounds [44–49]. To our knowledge, this type of chemistry has not been investigated in the specific context of metal NPs formation, so contamination of the NPs surface with non-identified species is a possibility. In short, it is desirable to obtain new polymeric structures endowed with functional groups that can reduce the metal ions with well-defined chemistry, without resorting to external reductants, high temperatures or radiation. Ideally, the oxidized functional groups on the polymer should also stabilize the growing NPs, thus enhancing their shelf life. Carboxylate groups are good candidates to this end [50–55].

The 2-(hydroxyimino)aldehyde (HIA) group (Fig. 1), which has been obtained through a facile synthesis in our laboratory, [56] can be viewed as both a metal ligand and a reductant, due to the presence of an oxime and an adjacent aldehyde moiety.

In our previous studies we used RAFT polymerization to obtain random and block copolymers of oligoethyleneglycol methacrylate and 2-(hydroxyamino)aldehyde butyl methacrylate (HIABMA). We have shown that, through a pH gradient technique, loose micelles are obtained from random copolymers and well-defined core–shell micelles from block copolymers [57]. In the presence of a base, pH- and temperature-responsive block copolymer pTEGMA-*b*-pHIABMA (Fig. 1), comprising a hydrophilic pTEGMA block and a hydrophobic pHIABMA chain, quantitatively and rapidly incorporates Cu^{2+} ions into pre-formed polymeric core–shell micelles (d = 20–25 nm) by complexation involving oximate ions [58]. As a result, we obtained a recyclable micellar system that uptakes and releases Cu^{2+} through pH or temperature changes. The main goal of the present work is to assess the performance of HIA-containing polymeric micelles as self-sufficient reducing nanoreactors for the formation of AgNPs. A similar approach has been recently described, in which Covalent Organic Frameworks were used as all-in-one reductants for Ag^+ and templates for ultra-small AgNPs growth [59]. We envisaged that Ag^+ may be taken up by the micelle core, where it may be reduced in alkaline conditions by the aldehyde group present in the HIABMA units. The carboxylate group resulting from aldehyde oxidation, together with the adjacent oxime group, would play a role in stabilizing the AgNPs. Furthermore, we surmised that loose and core–shell micelles may result in different sizes and/or arrangements of the micelle-embedded AgNPs. Thanks to their micellar assembly, the resulting materials may exhibit favorable properties including biocompatibility, *in vitro* and *in vivo* stability and ability to accumulate at the target site due to enhanced permeability and retention effect [60].

As an exploratory comparison of the *in vitro* antimicrobial performance of the obtained materials vs. literature examples, we determined their activity against gram-positive *Staphylococcus aureus* and gram-negative *Pseudomonas aeruginosa*.

2. Materials and methods

Gel Permeation Chromatography. GPC analyses were performed on a Hewlett Packard Series 1050 HPLC system equipped with a 1047A RI detector and a TSK gel alpha-4000 GPC column (Tosoh, Japan), using DMF with 0.1 % (w/w) LiBr as the mobile phase at a flow rate of 0.8 mL min^{-1}. The system was coupled to Clarity software version 6.2 (DataApex, Prague, The Czech Republic) for signal processing. Molecular weights are relative to monodisperse polyethylene oxide (PEO) standards (Agilent). The concentration of the polymeric solutions was ≈1 – 2 mg mL^{-1}. Samples were filtered through poly(vinylidene difluoride)

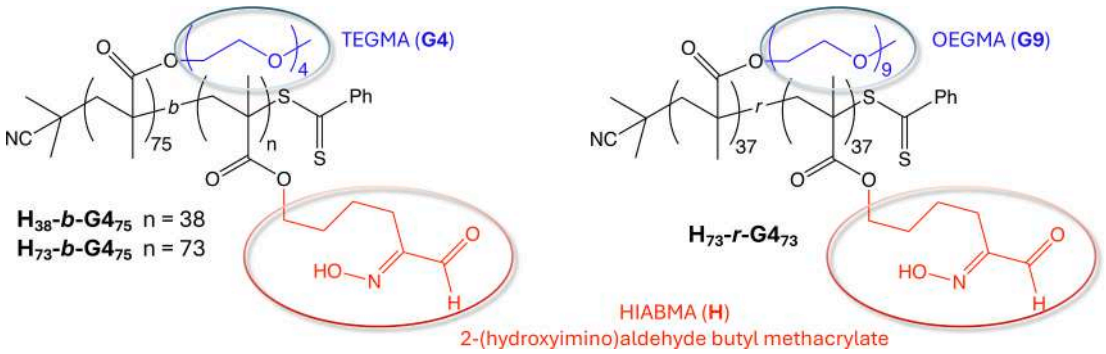

Fig. 1. Polymers used in this study. **Left**: Block copolymers with hydrophilic blocks of same composition (75 units of TEGMA: tetraethylene glycol methyl ether methacrylate) and two hydrophobic blocks of different lengths (38 and 73 units of HIABMA: 2-(hydroxyamino)aldehyde butyl methacrylate). **Right**: Random copolymer with 37 units of OEGMA (oligoethylene glycol methyl ether methacrylate with nine ethylene glycol units) and 37 HIABMA units.

(PVDF) syringe filters 0.45 μm, 13 mm (Lab Service, Italy) prior to analysis.

NMR Spectrometry. ^{1}H NMR and ^{13}C NMR spectra were recorded on a Bruker AVANCE 300 spectrometer (300 and 75 MHz), or Bruker AVANCE III 400 (400 and 100 MHz). Chemical shifts are referred to the residual solvent signal and expressed in parts per million (δ scale).

Dynamic Light Scattering. DLS data were obtained with a Brookhaven Instruments Corp. BI-200SM goniometer equipped with a BI-9000AT digital correlator using a solid-state laser (125 mW, $\lambda = 532$ nm). Measurements of scattered light were made at a scattering angle θ of 90°and at a temperature of 25.0 ± 0.1 °C. The experimental duration was in the range of 5 − 20 min, and each experiment was repeated two or more times. Cumulant analysis or CONTIN was used to fit the data.

UV − Vis Spectrophotometry. Spectra were recorded on a Varian Cary 50 Probe UV − vis spectrophotometer equipped with a cell-holder with an external water circulator for temperature control.

TEM measurements. Transmission electron microscopy analyses were carried out with a Tecnai 12 G2 Twin (ThermoFisher Scientific Inc), equipped with a lanthanum hexaboride thermionic electron source, operating at a primary beam maximum energy of 120 keV. Electron images and diffraction patterns were acquired with a 12 megapixels digital CMOS sensor (Emsis GmbH), installed in the projection chamber at the end of the magnetic lens column, which could be inserted on demand along the microscope optical axis above the viewing screen. Diffraction patterns were obtained by means of Nanoarea Electron Diffraction (NED), and the sample volume was directly selected using a highly collimated and coherent primary electron beam, controlled by condenser apertures and lenses. In this way, a very high spatial resolution could be achieved, with an electron beam diameter of a few tens of nanometers (about 30 nm). X-ray Energy Dispersive Spectrometry (XEDS) measurements were performed on a Thermo-Ultradry (ThermoFisher Scientific Inc), selecting the sample volume of interest by the same nanoarea electron beam method used in NED. Some other measurements were carried out with a JEOL JEM F200 operating at a primary beam maximum energy of 200 kV. Electron images and diffraction patterns were acquired with a Gatan Rio16 CMOS camera. All samples were prepared placing a suspension drop (5 μL) on a TEM 400 mesh Cu grid covered with a thin amorphous carbon film. Sometimes, to better visualize the polymeric particles, the negative staining was applied using phosphotungstic acid (PTA) aqueous solution 2 % w/v buffered at pH 7.3 with NaOH.

STEM measurements. STEM images were obtained using a ZEISS Auriga scanning electron microscope equipped with the STEM module for operation in transmission mode. The samples were deposited by drop casting on 400 mesh copper grid covered with a 20 nm amorphous carbon film (Agar Scientific) and loaded inside the electron microscope by the specific sample-holder. To get a good compromise between transmitted image resolution and low radiation damage, the electron beam was accelerated at 20 kV, while the working distance is set around 2 mm.

SAXS measurements. SAXS measurements were performed at SAXSLab Sapienza with a Xeuss 2.0 Q-Xoom system (Xenocs SA, Grenoble, France), equipped with a micro-focus Genix 3D X-ray source (λ = 0.1542 nm) and a two-dimensional Pilatus3 R 300 K detector (Dectris Ltd., Baden, Switzerland). The beam size was collimated to 0.5 mm x 0.5 mm and the calibration of the scattering vector module (q), where $q=(4\pi \sin\theta)/\lambda$, 2θ being the scattering angle, was performed using silver behenate. Measurements at three sample-detector distances were performed so that the overall explored q region was 0.04 $nm^{-1} < q < 12$ nm^{-1}. Samples were loaded into disposable borosilicate glass capillaries cells, sealed with hot glue and measured in the instrument sample chamber at reduced pressure (~0.4 mbar) at room temperature (23–25 °C). The two-dimensional scattering patterns were subtracted for the "dark" counts, and then masked, azimuthally averaged, and normalized for transmitted beam intensity, exposure time and subtended solid angle per pixel, by using the FoxTrot software developed at SOLEIL. The one-dimensional intensity vs. q profiles were then subtracted for the water and empty capillary contributions and put in absolute scale units (cm^{-1}) by dividing for the thickness close to 1.5 mm as estimated from the transmission scans. The different angular ranges were merged using the SAXS utilities tool [61]. Guinier fit analysis and the indirect Fourier transform to calculate the pair distance distribution functions were performed with the SAS Data Analysis tools of the ATSAS package [62]. Attempts to describe the sample scattering according to analytical models were performed with the software package Sasfit [63].

Synthesis of monomer and polymers. 4-[(hydroxyimino)aldehyde]butyl methacrylate (HIABMA) monomer and all the polymers were synthesized as previously described [57,64]. In this study we used two block copolymers and one random copolymer: **H_{38}-*b*-$G4_{75}$, H_{73}-*b*-$G4_{75}$** and **H_{37}-*r*-$G9_{37}$**, where **G4** is a tetra(ethyleneglycol)methyl ether methacrylate repeat unit and **G9** is oligo(ethyleneglycol)methyl ether methacrylate with about nine ethylene glycol units in the side chain. Subscript numbers represent the average degree of polymerization. Đ. (M_w/M_n, GPC) < 1.2 for all polymers.

2-(hydroxyimino)decanal. 2-(hydroxyimino)decanal was obtained by α-oximation reaction of decanal (Merck, ≥ 98 %) as previously described [56] under inert atmosphere using pyrrolidine (Merck, ≥ 99 %), *p*-toluenesulfonic acid monohydrate (*p*-TsOH; Merck, > 98 %), $NaNO_2$ (Merck, ≥ 99 %) and anhydrous $FeCl_3$ (Merck, > 97 % reagent grade) in anhydrous DMF (Merck, ≥ 99.8 %). The reaction was continued at room temperature for 5 h, and the product was isolated by extraction with ethyl acetate and subsequent purification on silica gel using a gradient of hexane/ethyl acetate. Yield was 59 %.

pH-induced micellization. Core-shell micelles were obtained from the copolymers as previously described [57]. MilliQ water (18.2 MOhm · cm) was used throughout the preparation. Briefly, the appropriate

amount of **H_{38}-*b*-G4$_{75}$**, **H_{73}-*b*-G4$_{75}$** or **H_{37}-*r*-G4$_{37}$** polymer ([HIA] = 2.2 x10^{-6} mol) was dissolved in 1 mL NaOH 0.1 M (prepared from NaOH pellets, Merck, ≥ 98 %). After stirring for 30 min, the solution became clear, and pH was 11. The pH was then gradually lowered by the addition of 0.1 M HCl (prepared from HCl puriss p.a. ≥ 37 %, Merck, ACS Reagent), and the formation of nanoaggregates was monitored by DLS. The final volume was adjusted to obtain [HIA] = 1.8x10^{-3} M.

Preparation of AgNPs in the pre-formed micelles. Experiments were performed by adding the appropriate aliquots of $AgNO_3$ (Merck, ≥ 99 %) or silver acetate AgOAc (Merck, synthesis grade) 0.05 M in milliQ water (18.2 MOhm · cm) under stirring to the micelles obtained by pH-induced micellization at [HIA] = 1.8 x 10^{-3} M. AgOAc was used in the experiments in which the absorption bands of the oxime (230 nm) or the oximate ion (280 nm) was compared, because nitrate anion has a strong absorption band in the 200–240 nm region. NaOH 0.1 M was added after silver ions. The final ratio was [HIA] / [Ag^+] / [NaOH] = 1:1:1. AgNP formation was monitored by UV–visible spectrophotometry.

Centrifugal filtration experiments. Centrifugal filtration experiments were conducted using an ALC 4236 centrifuge. Centricon SR3 filters with a cut-off of 30 kDa were used as filtration systems. Samples of 1–2 mL were centrifuged at a speed of 3000 rpm for 5–15 min as a function of the sample volume.

Antimicrobial susceptibility test. To test the biological activity of AgNPs, *Pseudomonas aeruginosa* ATCC 15692 and *Staphylococcus aureus* ATCC 25923 have been cultivated in Luria-Bertani (LB) medium: 1 % of tryptone (DifcoTM, USA), 0.5 % of yeast extract (DifcoTM, USA), 0.5 % of NaCl (Carlo Erba, Italy) and 1 mL/L of NaOH 1 N in ddH_2O. To prepare LB agar solid medium, 2.1 % of agar (DifcoTM, USA) was added. Bacterial strains were inoculated in LB broth and grown overnight (37 °C – 160 rpm) to reach the stationary phase. *P. aeruginosa and S. aureus* 5x10^5 cells/mL were collected and inoculated into LB medium. AgNPs were added to the bacterial strains to obtain 5.4 or 11 μg mL^{-1} final Ag^+ concentrations, with 21 and 42 μg mL^{-1} micelles, respectively. Metal-free-micelles of same concentrations were also tested for comparison. Upon overnight incubation at 37 °C with shaking (160 rpm), the bacterial growth was evaluated by reading absorbance at 600 nm through LLG-uniSPEC2 spectrophotometer (LLG, Germany) at different time points and compared to NP-free samples.

3. Results and discussion

3.1. Preparation of micelle-embedded AgNPs

In previous work [58], we demonstrated that micelles obtained by pH-induced micellization from the amphiphilic block copolymer **H_{38}-*b*-G4$_{75}$** (Fig. 1) can quantitatively and rapidly incorporate Cu^{2+} ions into the core by complexation involving oximate ions formed in the presence of a base. The entire procedure is carried out in aqueous solution without using organic solvents. The pKa of the HIA-Cu^{2+} complexes was determined by UV–Vis spectrometry, measuring the intensity of the oximate band at 280 nm as we titrated the solution with NaOH. In short, we demonstrated that oxime dissociation is necessary to form micelle–Cu^{2+} complexes and that Cu^{2+} complexation enhances the acidity of the oxime group by about six orders of magnitude, the apparent pKa of the oxime group being lowered from 11.3 to 4.7. In the present work, we aimed to obtain micelle-stabilized AgNPs by adapting this approach. Firstly, we checked whether addition of a base is necessary to incorporate Ag^+ into the polymeric micelles. Aqueous $AgNO_3$ was simply added to pre-formed micelles of **H_{38}-*b*-G4$_{75}$** copolymer (D_h = 30 nm by DLS; [HIA] = 1.8 x 10^{-3} M) at [HIA] / [Ag^+] = 1:1), and the mixture was submitted to centrifugal filtration (cut-off 30 kg/mol) to check for Ag^+ retention by the micelles. A white precipitate (AgCl; K_{ps} AgCl = 1.8 x 10^{-10} $mol^{-2}L^{-2}$) formed when HCl 0.1 M was added to the filtrate. The turbidity of the suspension, as determined at 500 nm, was similar to that observed in a polymer-free $AgNO_3$ solution of same concentration, thus indicating little or no Ag^+ retention by the polymeric micelles. Upon adding NaOH to a micelle-Ag^+ solution up to [HIA] / [Ag^+] / [NaOH] = 1:1:1, we did not observe any turbidity deriving from AgOH precipitation. Centrifugal filtration of this micellar solution immediately after the addition of NaOH afforded a clear colorless filtrate that did not turn cloudy upon the addition of HCl, indicating that nearly all Ag^+ ions had been bound to HIA. So, addition of a base is necessary to promote Ag^+ complexation. The formation of a white AgOH precipitate (K_{ps} AgOH = 2 x 10^{-8} $mol^{-2}L^{-2}$), that quickly became brown (**Fig. S1**), was evident, instead, after addition of NaOH to 1.8 x 10^{-3} M $AgNO_3$ ([NaOH] / [Ag^+] = 1:1). The same result was obtained with the **G4** homopolymer (**Fig. S1**), which mimics the micellar corona, so the presence of the HIA groups in **H_{38}-*b*-G4$_{75}$** micelles is necessary to stabilize Ag^+ in solution in alkaline conditions. Furthermore, a brown color developed over time with the **H_{38}-*b*-G4$_{75}$** micelles, and the solution remained clear and homogeneous for months. So, the HIA groups in the core of the **H_{38}-*b*-G4$_{75}$** micelles are key to obtaining a stable silver colloid. When AgOAc was used instead of $AgNO_3$ ([HIA] / [Ag^+] = 1:1), no significant absorbance developed around 280 nm (**Fig. S2)** indicating that acetate is a base not strong enough to deprotonate the HIA oxime. We then added a stoichiometric amount of NaOH ([HIA] / [Ag^+] / [NaOH] = 1:1:1) and we followed the evolution of the UV–Vis spectra over time (Fig. 2). The oximate band at 280 nm is initially observed as soon as the base is added to the Ag^+-micelle mixture, then its intensity decreases in favor of an additional broad band centered at 418 nm, corresponding to the brown color of the clear solution (inset in Fig. 2). The intensity of this band increases as a function of NaOH added to the [HIA] / [Ag^+] = 1:1 solution (**Fig. S3**).

The same experiment shown in Fig. 2 was conducted with micelles obtained from **H_{73}-*b*-G4$_{75}$**, a block copolymer having twice the HIA repeat units as **H_{38}-*b*-G4$_{75}$**, and with the random copolymer **H_{37}-*r*-G9$_{37}$**, endowed with longer PEO pendent chains. The spectral features and their evolution in time were similar to those of **H_{38}-*b*-G4$_{75}$ (Fig. S4).** As for the acid-base properties of the HIA groups in **H_{38}-*b*-G4$_{75}$** in the presence of the metal ion, the oximate band (280 nm) was persistent enough to allow us to titrate the HIA group with NaOH in the presence of an equimolar amount of $AgNO_3$. A non-linear fit of the experimental data results in an estimated pKa of 5.5 (**Fig. S5**). This value is more than five pKa units lower than that of **H_{38}-*b*-G4$_{75}$** pristine micelles (pKa ~ 11) and one unit higher than that of **H_{38}-*b*-G4$_{75}$** in presence of Cu^{2+}. Such significant dependence of the oxime acidity on the metal ion strongly suggests a specific interaction between the oximate group and Ag^+. The broad band at 418 nm shown in Fig. 2 **and S4** is compatible with either the spectral properties of Ag_2O, or with SPR of AgNPs. Douglas Gallardo et al [65]. tackled the issue of telling apart NPs of Ag_2O and Ag(0)

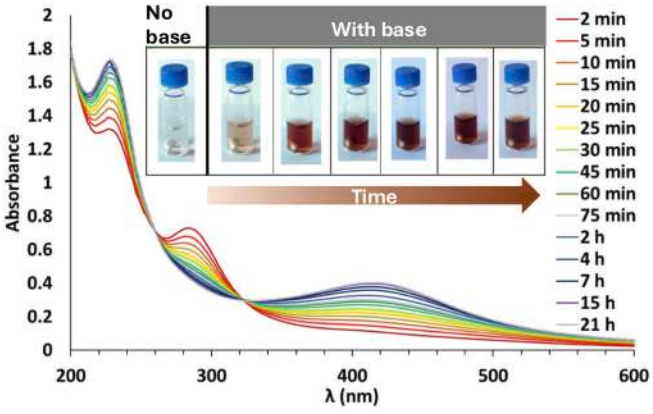

Fig. 2. Absorption spectra in water of **H_{38}-*b*-G4$_{75}$** pH-induced micelles, [HIA] = 1.8 x 10^{-3} M, in presence of silver acetate CH_3COOAg and NaOH ([HIA] / [Ag^+] / [NaOH] = 1:1:1), recorded as a function of time. Optical path length 0.1 cm. Solutions at different timepoints after NaOH addition are shown in the inset.

through well-known basic chemistry. Specifically, when treating Ag_2O with concentrated NH_3, colorless $[Ag(NH_3)_2]^+_{(aq)}$ is formed, whereas AgNPs do not change their spectral features with NH_3. Furthermore, Ag (0) is dissolved very slowly by HNO_3 upon oxidation to $AgNO_3$, while Ag_2O is readily attacked by the acid. In our silver-micelle system, we did not observe any change in color upon addition of NH_3. Furthermore, it took 30 days from addition of HNO_3 for the solution to become colorless (**Fig. S6**). We thereby surmised that not only do the deprotonated HIA groups in **H_{38}-*b*-$G4_{75}$** trap Ag^+ in the micelle core, but they also reduce the metal ion to afford stabilized AgNPs with no need for an external reductant (Fig. 3).

As a result, the acidity of the oxime decreases as the oximate-Ag^+ interaction is disrupted by metal reduction, oximate ions are thereby protonated, and the intensity of the 280 nm band decreases accordingly. The two isosbestic points observed in Fig. 2 correspond to the concomitant formation of AgNPs (increase of the 418 nm band) with re-protonation of the oxime (decrease of 280 nm band and increase at 230 nm). Our assumption was that the aldehyde moiety in the HIA group be accountable for the reduction of Ag^+ in the presence of a base [66,67], to yield the corresponding 2-(hydroxyimmino)carboxylate. To verify our assumption, we investigated this reaction independently by ^{1}H NMR on a simplified model for the HIABMA repeat unit, i.e. 2-(hydroxyimino) decanal (Fig. 4**A**). No functional groups other than HIA are present in this model structure, so this experiment allowed us to single out its reactivity towards Ag^+.

The reaction was carried out on a small scale in the NMR tube and, 2-(hydroxyimino)decanal being water-insoluble, CD_3OD was used as the reaction solvent. [67] First, a 2:1 M ratio of $AgNO_3$ was added to the HIA solution. The position of the –C*H*O signal remained unchanged upon addition of Ag^+ (δ = 9.38 ppm. Fig. 4**B**). However, its intensity was halved to the benefit of a singlet at δ = 5.05 ppm, attributed to the hemiacetal form of the aldehyde (**Fig. S7** for structural elucidation by ^{13}C and 2D NMR), which forms in methanol with Ag^+ acting as Lewis acid catalyst. When NaOH was also added (HIA / Ag^+ / OH^- = 1:2:2), a brown-black precipitate and a silver film inside the NMR tube formed immediately, the –C*H*O peak was almost entirely suppressed (Fig. 4**C**) and no additional signal of corresponding intensity appeared this time. ^{13}C NMR (See **Fig. S8**) confirms the oxidation of the aldehyde moiety to carboxylate [68]. Furthermore, no deoximation reaction occurred, since the > *C*NOH signal (153.68 ppm in **Fig. S8**) is still present in the product and no peaks are detected in the ketone range (>190 ppm). The entire reaction sequence is outlined in Scheme 1 for both the model molecule in CD_3OD, and the HIA groups in the aqueous micelle environment (**Fig. S8**).

Based on the work by Gomes et al. [67], the reducing species can be assumed to be the alkoxide resulting from deprotonation of the hemiacetal (in methanol) or aldehyde hydrate (in water). However, the most acidic group in HIAs is the oxime, so an additional prototropic equilibrium is required for Ag^+ reduction to take place (Scheme 1). DLS analysis of **H_{38}-*b*-$G4_{75}$** and **H_{73}-*b*-$G4_{75}$** micelles before and after the formation of AgNPs does not show any significant difference in their diameter (Fig. 5**)** indicating that AgNP formation does not entail relevant micelles swelling or disassembling.

TEM analysis was used to characterize size and morphology of AgNPs. With no staining**,** Fig. 6**a and c** show groups of 2 nm AgNPs. Image analysis confirms AgNPs size distribution spanning 1–3 nm, the most populated diameters being 2 nm. Negative staining with phosphotungstic acid (Fig. 6**c and d**) shows dark AgNPs distributed throughout the white domains resulting from the polymeric micelles. These are about 10–20 nm diameter with **H_{38}-*b*-$G4_{75}$**, somewhat larger with **H_{73}-*b*-$G4_{75}$.**These values appear significantly smaller with respect to the sizes determined by DLS (30–40 nm). It is possible that the drying of the samples for TEM analysis causes the pOEGMA corona to fold onto the pHIABMA core or to flatten on the TEM grid and be covered by the stain, so that TEM visualization underestimates the diameter of the polymeric aggregates. On a final note, AgNPs are more numerous with **H_{73}-*b*-$G4_{75}$** than with **H_{38}-*b*-$G4_{75}$**. This is reasonably due to the larger number of HIA units, leading to incorporation and reduction of more silver ions. Unfortunately, we have not been able to obtain a NED diffraction pattern, due to the small size of the AgNPs formed in the block copolymer micelles and because of the presence of the amorphous polymers and carbon film of the TEM grid.

The same AgNPs preparation procedure was also applied to the random copolymer **H_{37}-*r*-$G9_{37}$**. The longer PEO chains in the random copolymer (nine EG units instead of four) are necessary to ensure stability of the loose micelles in water [57]. **H_{37}-*r*-$G9_{37}$** nanoaggregates, prior to AgNPs formation, have an average D_H (DLS) of about 60 nm with high polydispersity (data not shown), consistent with the TEM images (negative PTA staining), which show an average diameter of about 40 nm (**Fig. S8a, b and c**). AgNPs formed with the random copolymer are larger than those obtained with the block copolymers, with an average diameter of about 10 nm (Fig. 7 and **Fig. S8a, b**), and they do not appear to be clustered.

In fact, unlike AgNPs formed within the block copolymers micelles, TEM with negative PTA staining (**Fig. S8d**) shows isolated AgNPs that are either surrounded by a thin **H_{37}-*r*-$G9_{37}$** polymer layer, or embedded into disorderly polymeric aggregates. So, block and random copolymers stabilize very small-sized AgNPs of somewhat different dimensions and spatial distribution. Owing to their larger diameter, a reasonable NED pattern was obtained for the 10 nm AgNP formed with **H_{37}-*r*-$G9_{37}$** (Fig. 7c). The main reflection gave interplanar distances of 2.327, 2.084, 1.479 and 1.255 Å corresponding to the (111), (200), (220) and (311) planes of face-centered cubic (fcc) metallic silver.

H_{38}-*b*-$G4_{75}$ micelles were investigated by SAXS in solution before and after AgNP formation (Fig. 8). The unloaded micelles can be described as spherical aggregates with maximum size of 29.5 ± 0.5, and a non-sharp interface, in which the outer shell notably contributes as the scattering of random coils (Fig. 8**c**, **Table S1**), consistently with our previous study [58]. Following the simplified assumption that the pHIA blocks only populate the internal compact core (according to their insoluble nature at neutral pH), while the pOEGMA blocks only contribute to the outer shell scattering, the volume and electron densities of the two different blocks were calculated according to their chemical composition and fixed. However, the predicted scattering length densities are not different enough to reliably distinguish core and shell just based on their SAXS contrast, due to the similar chemical composition of the blocks (as also perceived by the rather smooth and monomodal pair distance distribution function Fig. 6**b**, **Figure S7a**),

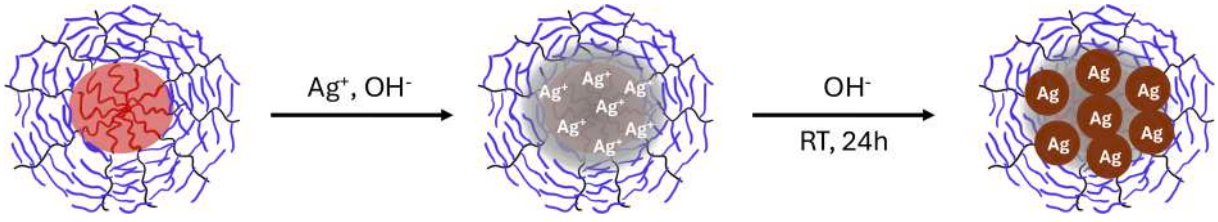

Fig. 3. Incorporation of Ag^+ in alkaline conditions within the pre-formed core–shell micelles of **H_{38}-*b*-$G4_{75}$** or **H_{73}-*b*-$G4_{75}$**. AgNPs grow within the micelle as a result of the reactions described in Scheme 1.

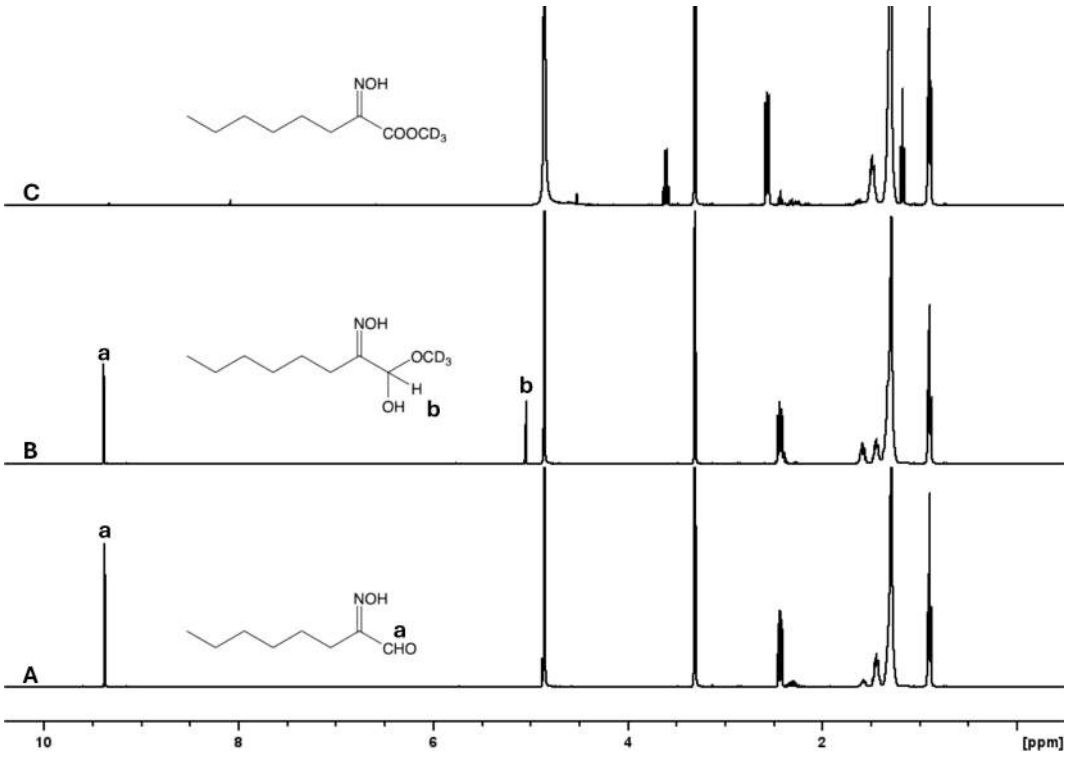

Fig. 4. ^{1}H NMR spectra in CD_3OD (solvent residual proton δ = 3.31 ppm) of **A.** 2-(hydroxyimino)decanal (–C*H*O δ = 9.38 ppm); **B.** hemiacetal form (–C*H*(OH)(OCD_3) δ = 5.05 ppm with HIA / Ag^+ = 1:2; **C.** Methyl carboxylate obtained with HIA / Ag^+ / OH^- = 1:2:2. Structures elucidation by ^{13}C and HSQC NMR in the Supporting Information.

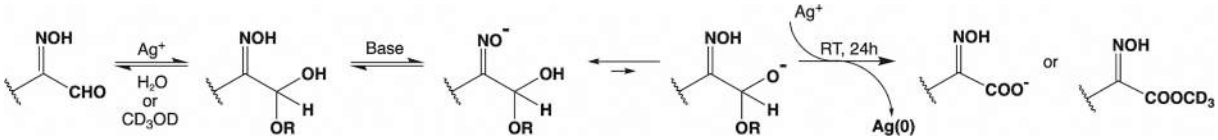

Scheme 1. Plausible reaction sequence between HIA groups and Ag^+ ions in alkaline water or alcohol, leading to oxidation of the aldehyde group to carboxylic function and reduction of silver ions to metallic Ag. A detailed discussion of the reduction mechanism can be found in Gomez et al.[68].

while the quantitative contribution of the outer disordered polymer shell appear robust, being necessary to reasonably fit the data.

In the AgNPs-loaded micelles, the scattering data clearly show a 7-fold increase of the intensity extrapolated at zero angle compared to the unloaded micelles, while the overall size is not significantly modified, as detected by values of the radius of gyration close to 8.6 nm (inset of Fig. 8**a**) and a maximum distance in the pair distance distribution function of 30 nm (Fig. 8**b**). Also, by looking at the normalized pair distance distribution functions (**Fig. S10a**) it can be observed that the distance of maximum probability is shifted to slightly lower sizes in the AgNPs-micelle sample (8 nm) compared to the pristine sample (10 nm). These model-independent observations already agree with an overall increase of the electron density contrast of the spherical polymer aggregates as electron rich atoms of Ag are incorporated, and with a preferential growth in the inner portion of the polymer aggregate rather than at the surface.

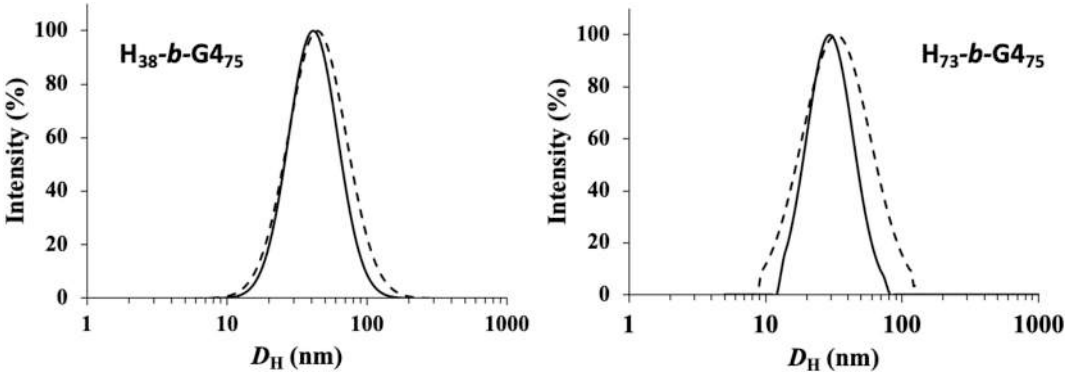

Fig. 5. Size distribution obtained using the CONTIN analysis for DLS measurements in water of (left) $\mathbf{H_{38}}$-***b***-$\mathbf{G4_{75}}$ and (right) $\mathbf{H_{73}}$-***b***-$\mathbf{G4_{75}}$ micelles, before (full line) and after (dashed line) AgNP formation (24 h). [HIA] = 1.8 x 10^{-3} M; [HIA] / [$AgNO_3$] / [NaOH] = 1:1:1.

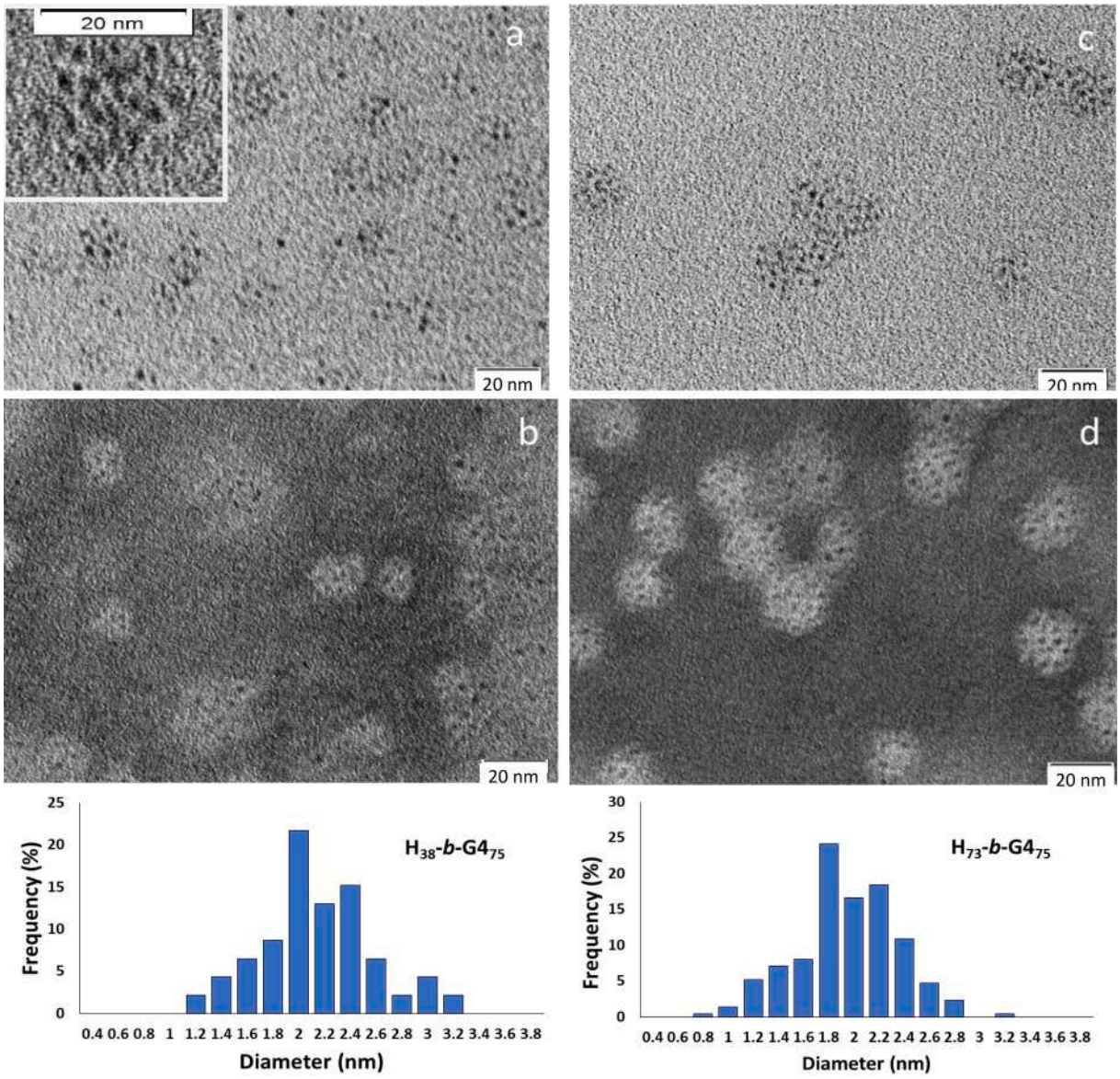

Fig. 6. TEM images of AgNPs and size distributions obtained by TEM images analysis. AgNP-$\mathbf{H_{38}}$-***b***-$\mathbf{G4_{75}}$ without (a) and with (b) PTA contrast agent. AgNP-$\mathbf{H_{73}}$-***b***-$\mathbf{G4_{75}}$ without (c) and with (d) PTA contrast agent. Composition: Micelles in aqueous solutions of [HIA] / [Ag^{+}] / [NaOH] = 1:1:1, [HIA] = 1.8 x 10^{-3} M.

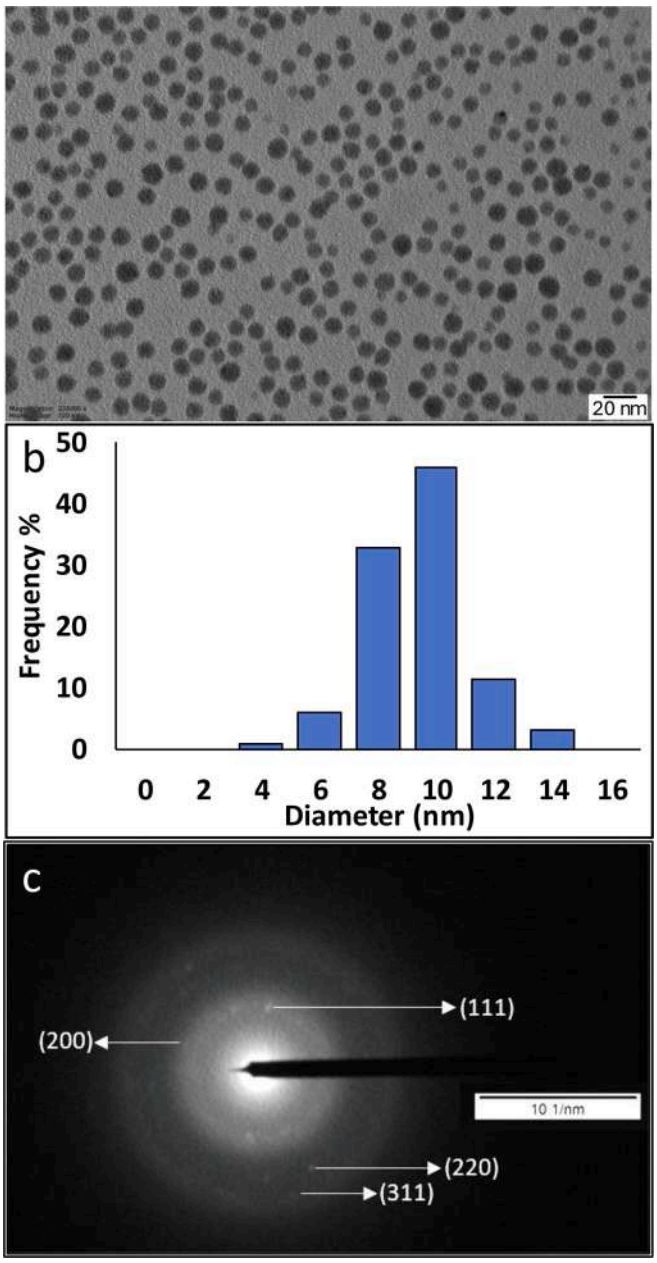

Fig. 7. TEM image of AgNP formed in presence of H_{37}-*r*-$G9_{37}$ nanoparticles, [HIA] / [Ag^+] / NaOH] = 1:1:1, [HIA] = 1.8 x 10^{-3} M (a), size distribution obtained by TEM image analysis of the AgNP (b), electron diffraction pattern obtained by NED (c).

For the sample in which AgNPs were formed, a more careful inspection of the scattering profile at larger q values suggests an additional Guinier region in the range 1.5–2.5 nm^{-1}, corresponding to electron density inhomogeneities with R_g of approximately 0.6 nm and maximum diameter of 1.8 nm (inset of Fig. 8**c**, Fig. 8**d**). It is therefore highly likely that the SAXS signal for $q > 1.5$ nm^{-1} arises from the nucleated AgNPs also detected in the TEM micrographs and can be fitted as spheres with radius 0.785 ± 0.012 nm (dotted red line in Fig. 8c, Table S1). The scattering length density difference ($48{\cdot}10^{-4}$ nm^{-2}) and the number concentration ($104{\cdot}10^{-7}$ nm^{-3}) of the model intensity on absolute scale are compatible within 10 % with the known concentration of 1.8 x 10^{-3} M Ag packed with density of 7.9 $g{\cdot}cm^{-3}$, as the average value reported in the literature for nanoparticles (Table S1, Table S2) [69].

However, the fact that the overall SAXS data cannot be described by a simple sum of the scattering of the small AgNPs (that mainly contribute to the experimental SAXS intensity I(q) for $q > 1.5$ nm^{-1}) and of the pre-existing polymer micelles (that have a much lower scattering contrast due to their chemical composition), but rather imply a much higher intensity in the low q (**Fig. S10b**), strongly supports that the AgNPs are not free from the polymer micelles but are embedded in these larger spherical particles and their positions are correlated to give the overall scattering signal.

To obtain an estimate of the average number of AgNPs embedded within one polymer micelle, we recalled the equation for the scattering of a "dirty snowball" object [70] developed from the Debye formula assuming a collection of *n* small monodisperse spheres within a large spherical particle, but considered only its value extrapolated at zero angle, where all excess electrons should scatter in phase (see Supporting information Equation 1 and Table S2). This calculation measures 20 ± 1 small AgNPs with radius 0.785 nm inside each large spherical particle of radius 9.68 nm, in agreement with the estimate based on the expected stoichiometry and known concentration. This result is also compatible with the TEM micrographs.

To describe the overall SAXS signal a tentative analytical model for the structure factor was applied, in combination with form factor of the small Ag spheres fitting the data at $q > 1.5$ nm^{-1} as described before. A reasonable best-fit agreement was obtained considering globular clusters with a correlation length ξ of 4.7 nm (corresponding to a correlation volume of $8\pi\xi^3 = 2613$ nm^3, i.e. with spherical radius of 8.5 nm). Therefore, the SAXS data agree with the model of 2-nm sized AgNPs grown within the interior of the polymer micelles, to form spherical clusters comprising approximately 20 nanoparticles each, with diameter of the order of 20 nm, slightly smaller than the maximum size of the entire polymer micelle.

The different outcomes in AgNPs formation in the loose micelles formed by **H_{37}-*r*-$G9_{37}$** and in the core–shell micelles formed by **H_{38}-*b*-$G4_{75}$** can be rationalized in view of the reduction mechanism outlined in Fig. 4. Nucleation of the AgNPs is controlled by the distribution of the HIA groups across the micellar nanoreactor, by the mobility of the growing NPs, and by the composition of the nanoenvironment. In the well-segregated core of the micelles obtained from the block copolymer, AgNPs grow in a medium that is virtually PEG-free and quite dehydrated, so their coalescence is prevented by capping with the oxime and carboxylate groups, thus stabilizing the clusters of ultra-small particles. In the loose micelles obtained from the random copolymer, PEG and water are present nearby the nucleation sites, and NP growth occurs similarly to other polymeric systems, yielding larger single colloidal particles of low dispersity. It should be noted that, in our previous study [57] we showed how different compositions of the block copolymers lead to micelles with different structures, which may also result in AgNPs of various size and arrangement. Therefore, specific applicative needs may be met by this system.

As for the long-term stability of the AgNPs, no changes in the UV–Vis spectra and DLS distribution were observed over a six-month period at room temperature with any of the samples. TEM analysis of the AgNP / **H_{38}-*b*-$G4_{75}$** sample after 20 months at 4 °C (**Fig. S11**) still shows clusters of ultra-small AgNPs, with no evidence of coalescence. The contrast, however, is much lower with respect to the initial TEM images (Fig. 6**a**), due to partial solubilization of Ag^+. This observation indicates that, once the AgNPs are formed within the micellar nanoreactors, their morphology is stable over a long period of time, even as Ag^+ is released in the aqueous environment.

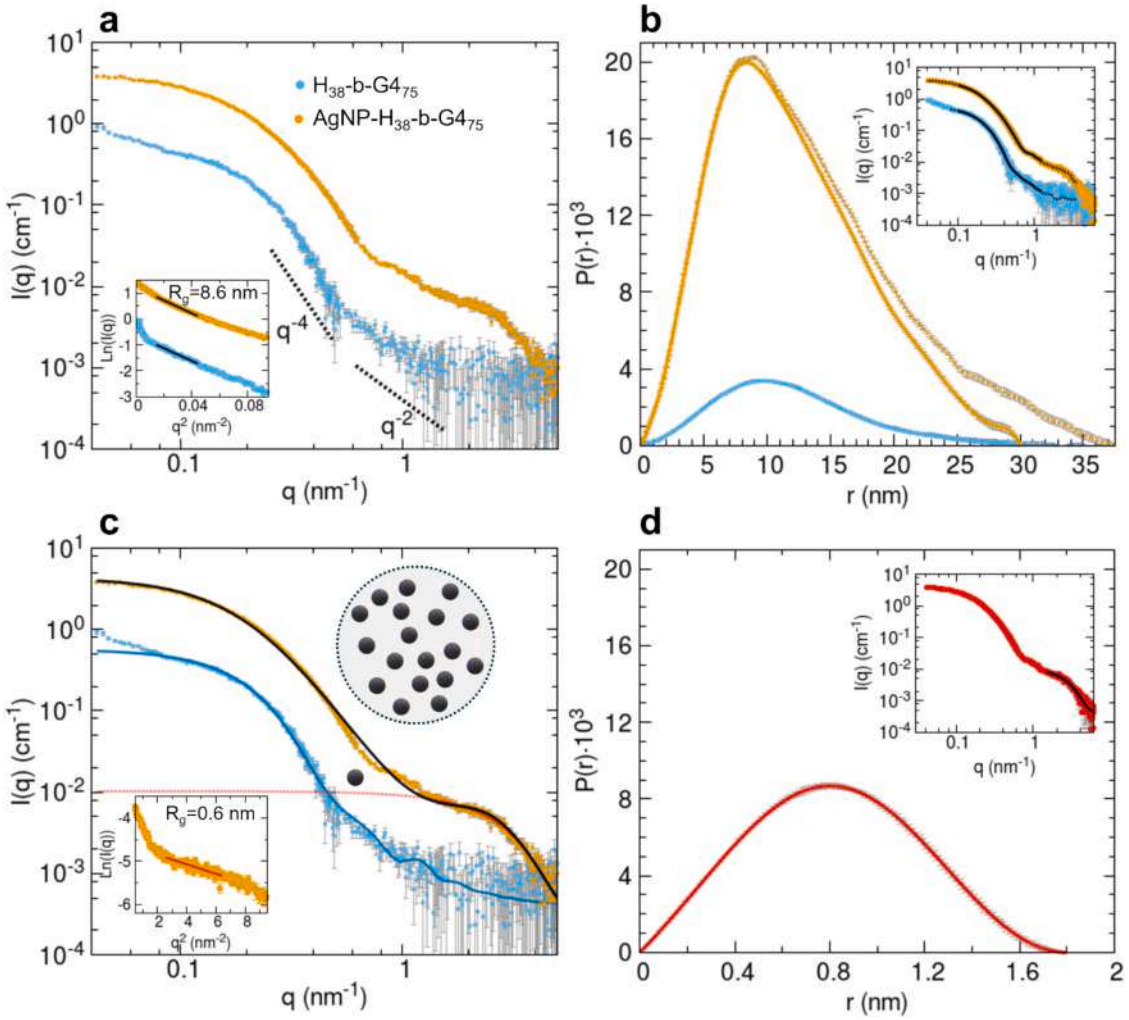

Fig. 8. a) SAXS profiles of the polymeric micelles sample (**H_{38}-*b*-$G4_{75}$**) before and after addition of NaOH and $AgNO_3$ ([Ag^+] / [HIA] = 1:1), with characteristic power laws displayed for comparison and the Guinier fits in the q range 0.11–0.21 nm^{-1} shown in the inset. **b)** Pair distance distribution functions obtained by indirect Fourier transform of the SAXS data, with corresponding fits reported in the inset. The profiles shown as dotted lines were obtained by including a more extended portion of the experimental q range. **c)** Model profiles compared to the experimental SAXS data: form factor of a block copolymer spherical micelle (parameters reported in Table S1) for the Ag-free sample (blue line on cyan data points), spherical particles with radius of 0.785 nm for the AgNPs-micelles sample at $q > 1.5$ nm^{-1} (red dotted line on orange data points) and their tentative clustering model (black line on orange data points). In the inset, the Guinier fit for the AgNPs-micelles sample at $q > 1.5$ nm^{-1} is reported. **d)** Pair distance distribution functions obtained by indirect Fourier transform of the SAXS data of the AgNPs-micelles sample at $q > 1.5$ nm^{-1}, with the corresponding fit reported in the inset.

3.2. *Microbiological activity of the AgNPs*

The activity of AgNPs formed with **H_{38}-*b*-$G4_{75}$** micelles was tested in bacterial model systems, the Gram-positive *Staphylococcus aureus*, and the Gram-negative *Pseudomonas aeruginosa*. The effect of AgNPs on *S. aureus* after 20 h of growth is reported in Fig. 9**A**. Compared to the control, the percentage of growth after the overnight incubation stays below 10 % for both concentrations (9 % and 3 % ± 3 %, respectively). However, the activity of AgNPs on *S. aureus* is bacteriostatic because after 48 h of growth the bacterial cells reach the stationary phase (Fig. 9**B;** standard deviations ≤ 3 %). Micelles at 42 μg mL^{-1} without Ag slightly slow the achievement of the stationary phase. On *P. aeruginosa*, at 21 μg mL^{-1} the effect of the AgNPs is slightly bacteriostatic (Fig. 9**C:** 62 ± 13 % growth vs. control; Fig. 9**D:** same as control at 48 h), while at 42 μg mL^{-1}, the AgNPs exhibit bactericidal activity (Fig. 9**C and 9D:** < 2 % growth vs. control at 20 h and 48 h.).

Preliminary results on the antimicrobial activity of the micelle-embedded 2 nm AgNPs clusters are consistent with findings from other studies involving ultra-small polymer-based AgNPs, although direct comparisons must be made with caution due to differences in experimental conditions and strains used. Table 1 provides a frame of reference from recent literature examples on small (10–40 nm as an arbitrary interval) and ultra-small (2–10 nm) AgNPs, and even silver nanoclusters (AgNCs, < 2 nm).

Besides the differences in the microbiological assays and microbial strains, it should be noted that other active chemical species may be present in the formulations in Table 1, depending on synthesis and purification. It is, therefore, quite tricky to carry out a fair comparison between systems or to single out the role of AgNPs shape and size. Although, generally speaking, *P. aeruginosa* is considered more resistant, some studies report higher activity of AgNPs against Gram-negative bacteria, consistently with our results [79,80]. This likely depends on the AgNPs action mechanisms, which includes interaction with the bacterial surface – structurally different in Gram-positive and Gram-negative species. However, the AgNPs fabrication method may also be relevant. Arokiyaraj et al [81]. reported similar IC_{50} values of 7.5 μg ml^{-1} for both *Pseudomonas aeruginosa* and *Staphylococcus aureus*, with AgNPs of 121 nm diameter. In another study comparing the effects of AgNPs on reference and nosocomial strains of *P. aeruginosa*, Salomoni et al. found that 5 μg ml^{-1} of 10 nm AgNP was bactericidal [82]. In Liu

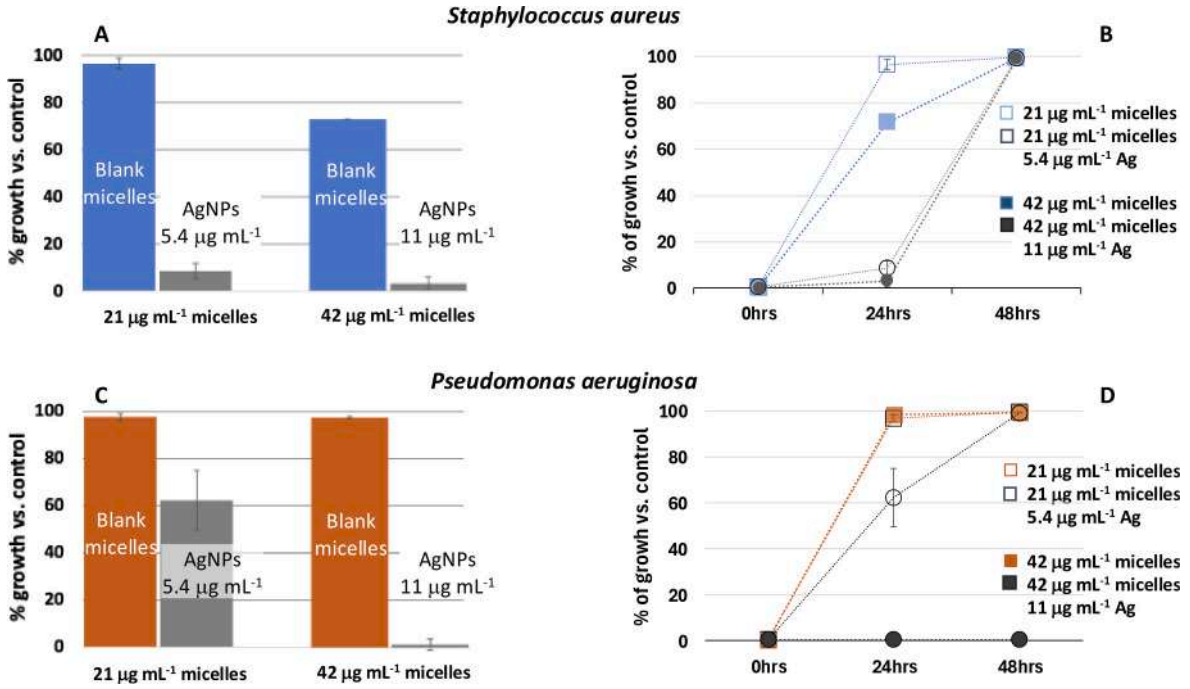

Fig. 9. Biological activity of AgNPs on *S. aureus* (A, B) and *P. aeruginosa* strains (C, D) treated with AgNPs 5.4 μg mL^{-1} and 11 μg mL^{-1}, with **H38-*b*-G4$_{75}$** micelles 21 and 42 μg mL^{-1}, respectively. % growth vs. control was determined by optical density at 600 nm. A and C: Comparison of activity on *S. aureus* and *P. aeruginosa* after 20 h of growth of Ag-loaded micelles and of metal-free polymeric micelles of same polymeric concentration. B and D: Growth curves of *S. aureus* and *P. aeruginosa* treated with Ag-loaded micelles and metal-free polymeric micelles of same polymeric concentration. After 48 h *S. aureus* reaches the stationary phase, indicating a bacteriostatic effect of both the AgNPs concentrations (B). On *P. aeruginosa* AgNPs shows a bactericidal effect at 1.8 μg mL^{-1} (D). Metal-free micelles exhibit negligible effect on both strains. Results are derived from 3 biological tests.

Table 1
Recent examples of AgNPs obtained with different methods and their activity against S. aureus *and* P. aeruginosa. *Results on other microorganisms not shown.*

Type of synthesis	Reducing agent	Stabilizing / capping agent	Particle shape	Average particle size[(a)]	Method	Results[(a)]	Ref.
Electrochemical	Electric arc	Carbon shell	Spherical	17 nm	MIC	*P. aeruginosa* – MIC 2 μg ml^{-1}	[71]
Green	*Pandanus tectorius* aerial root		Spherical	<30 nm	Disc diffusion assay	*S. aureus, P. aeruginosa* – at 30 μg ml^{-1} ZOI < 12.5 mm	[72]
Green	*Rubus discolor* leaves extract		Spherical	37 nm	Disc diffusion assay	*P. aeruginosa* – at 1 μg ml^{-1} ZOI = 18 mm	[73]
					MIC	*P. aeruginosa* – 0.83 mg ml^{-1}	
Green	Citrus peel extracts (various)		Spherical	2–4 nm	MIC	*S. aureus* – 16–63 μg ml^{-1}	[74]
Chemical	Reducing Covalent Organic Frameworks (COF)		Spherical	7–8 nm	Disc diffusion assay	*S. aureus, P. aeruginosa* – at 30 μg ml^{-1} ZOI = 13 mm	[59]
Chemical	$NaBH_4$	PVA/PVP (polyvinylalcohol/ polyvinylpyrrolidone)	Spherical	15–30 nm	Disc diffusion assay	*S. aureus* – 10–30 μl AgNPs suspensions. ZOI = 7 mm	[75]
Chemical	GSH/$NaBH_4$	Liposomes		< 2 nm	IC_{50}	*S. aureus* – 64 μM (Ag), *P. aeruginosa* 98 μM (Ag)	[76]
Chemical	Trisodium citrate	Trisodium citrate	Crystalline	63 nm	Disc diffusion assay	*P. aeruginosa*– at 2–8 mg ml^{-1} ZOI < 10 mm	[77]
Chemical	Glucose / NaOH	CTAB	Spherical/ cuboidal	85 nm	MIC	*S. aureus* – 0.003 μM	[78]
Chemical		PVP	Spherical	39 nm	MIC	*S. aureus* – 0.125 μM	[78]

[(a)] Particle sizes and concentrations may refer to Ag-only or Ag-containing assembly. Detail should be found in the specific references.
MIC = Minimum Inhibitory Concentration; ZOI = Zone of Inhibition

et al., [76] the IC_{50} of liposomial formulations of AgNCs (Table 1) was significantly higher for *P. aeruginosa* than for *S. aureus*. As for the present investigation, results in Fig. 9 are a preliminary assessment aimed at identifying the potential range of biologically active concentrations. These initial results make it worthwhile to carry out further detailed microbiological studies, also considering other microorganisms, which will include the accurate determination of MIC/MBC values and the clarification of the mechanism of action of both the single 10 nm, and the clustered 2 nm AgNPs. The micellar nature of our system may also provide the opportunity for the co-delivery of conventional antibiotics, which may act synergistically with the AgNPs. [83] Cytotoxicity of the formulations should also be taken into account in future studies.

4. Conclusions

Ultra-small AgNPs have been fabricated by reduction of Ag^+ within micelles obtained through a pH-gradient technique (pH-induced micellization) from copolymers of 4-[(hydroxyimino)aldehyde]butyl methacrylate and tetra- or oligo(ethylene glycol) methyl ether methacrylate. Reduction is achieved by the built-in aldehyde groups with no need for external reductants, high temperature or radiation. The entire process is highly sustainable, since polymer synthesis is conducted in DMSO (a benign solvent), micellization is pH-driven and does not require organic solvents, and no purification step is needed after AgNPs formation. Single spherical AgNPs (d = 10 nm) are obtained within the loose micelles fabricated with a random copolymer. Interestingly, ultra-small AgNPs (about 2 nm diameter) are formed in clusters within the core–shell micelles resulting from block copolymers. These differences in the nucleation of the AgNPs are rationalized in terms of distribution of the reacting functional groups, PEG chains and water across the micelle. All obtained AgNPs exhibit plasmonic resonance. The UV–Vis spectra and the size of the silver-loaded micelles (DLS) remain unaltered upon storage of the samples at room temperature for approximately six months. Furthermore, TEM analysis shows that the clustered distribution of the AgNPs in the block copolymer micelles is persistent even after 20 months at 4 °C, while Ag^+ was being released. Preliminary results of the antimicrobial activity of the micelle-embedded 2 nm AgNPs are in line with other ultra-small AgNPs-polymer systems. Further in-depth microbiological evaluation is in order to highlight any specificity of the system described in this work, also towards other microorganisms, and to elucidate its mechanism of action. The possibility to control the size and arrangement of the AgNPs through systematic changes in polymer composition and architecture may be of interest in fields such as fabrication of optical materials, metamaterials and nanoarchitectonics.

CRediT authorship contribution statement

Giancarlo Masci: Writing – review & editing, Writing – original draft, Supervision, Methodology, Investigation, Data curation, Conceptualization. **Francesca D'Acunzo:** Writing – review & editing, Writing – original draft, Methodology, Investigation, Conceptualization. **Stefano Casciardi:** Investigation. **Angela Cirigliano:** Investigation. **Alessandra Del Giudice:** Writing – original draft, Investigation, Formal analysis. **Francesco Mura:** Investigation. **Elena Passarini:** Investigation. **Emily Schifano:** Investigation. **Gabriella Maria Pastore:** Investigation. **Carlotta Petrianni:** Investigation. **Patrizia Gentili:** Writing – original draft, Methodology.

Declaration of competing interest

The authors declare that they have no known competing financial interests or personal relationships that could have appeared to influence the work reported in this paper.

Acknowledgements

The Authors acknowledge funding from:

GM and FD "Biomimetic antimicrobial vesicle-like nanoarchitectures for multi-drug-resistant bacteria—BELIEVE" Project funded by the European Union—NextGenerationEU under the National Recovery and Resilience Plan (NRRP), Mission 4, Component C2, Investment 1.1, Ministry of University and Research (MUR), Italy "Research Projects of Significant National Interest" (PRIN), Project code 2022HSFEPY, CUP B53D23013710006.

FD "One Health Basic and Translational Research Actions addressing Unmet Needs on Emerging Infectious Diseases - INFACT" - PE00000007, CUP B53C20040570005 NextGenerationEU, Project funded by the Ministry of University and Research (MUR), Italy under the National Recovery and Resilience Plan (NRRP) funded by the European Union

GM and PG "Chemistry for a Sustainable Development: new strategies for renewable fuels, removal of environmental pollutants and development of ecofriendly drugs to fight antimicrobial resistance and biofouling" – Departmental Project - Sapienza University of Rome, Italy Call 2023 – Project code RD12318AAD1CD97A

The Sapienza Research Infrastructure is acknowledged for the SAXS measurements at SAXSLab Sapienza, funded by the Large Equipment Project 2015-C26J15BX54. The authors would like to thank Prof. Antonio D'Alessandro, Director of the Centre of Nanotechnologies Applied to Engineering–CNIS, Sapienza University of Rome for access to the electron microscopy facility.

Appendix A. Supplementary data

Supplementary data to this article can be found online at https://doi.org/10.1016/j.eurpolymj.2025.114147.

Data availability

Data will be made available on request.

References

[1] A. Sati, T.N. Ranade, S.N. Mali, H.K. Ahmad Yasin, A.S. Pratap, Nanoparticles (AgNPs): Comprehensive Insights into Bio, Synthesis, Key Influencing Factors, Multifaceted Applications, and Toxicity—A,, Update, ACS Omega. American Chemical Society 2025 (2024), https://doi.org/10.1021/acsomega.4c11045.

[2] Capelli, D.; Scognamiglio, V.; Montanari, R. Surface Plasmon Resonance Technology: Recent Advances, Applications and Experimental Cases. *TrAC - Trends in Analytical Chemistry*. Elsevier B.V. June 1, 2023. doi: 10.1016/j.trac.2023.117079.

[3] H. Kang, J.T. Buchman, R.S. Rodriguez, H.L. Ring, J. He, K.C. Bantz, C.L. Haynes, Stabilization of silver and Gold Nanoparticles: Preservation and Improvement of Plasmonic Functionalities, Chem. Rev. 119 (1) (2019) 664–699, https://doi.org/10.1021/acs.chemrev.8b00341.

[4] J.R. Mejía-Salazar, O.N. Oliveira, Plasmonic Nanoarchitectured Systems for Biomedical Application, Adv. Colloid Interface Sci. 342 (2025) 103520, https://doi.org/10.1016/J.CIS.2025.103520.

[5] A. Taleb, C. Petit, M.P. Pileni, Optical Properties of Self-Assembled 2D and 3D Superlattices of Silver Nanoparticles, J. Phys. Chem. B 102 (12) (1998) 2214–2220, https://doi.org/10.1021/JP972807S.

[6] Y. Hang, A. Wang, N. Wu, Plasmonic Silver and Gold Nanoparticles: Shape- and Structure-Modulated Plasmonic Functionality for Point-of-Caring Sensing, Bio-Imaging and Medical Therapy, Chem. Soc. Rev. 53 (6) (2024) 2932–2971, https://doi.org/10.1039/D3CS00793F.

[7] S. Agnihotri, S. Mukherji, S. Mukherji, Size-Controlled Silver Nanoparticles Synthesized over the Range 5–100 Nm using the same Protocol and their Antibacterial Efficacy, RSC Adv. 4 (8) (2013) 3974–3983, https://doi.org/10.1039/C3RA44507K.

[8] B.J. Wiley, S.H. Im, Z.Y. Li, J. McLellan, A. Siekkinen, Y. Xia, Maneuvering the Surface Plasmon Resonance of Silver Nanostructures through Shape-Controlled Synthesis, J. Phys. Chem. B 110 (32) (2006) 15666–15675, https://doi.org/10.1021/JP0608628.

[9] K. Cao, X. Ge, S. Li, Z. Tian, S. Cui, G. Guo, L. Yang, X. Li, Y. Wang, S. Bai, Q. Wei, W. Li, Facile Preparation of a 3D RGO/g-C3N4 Nanocomposite Loaded with Ag NPs for Photocatalytic Degradation, RSC Adv. 15 (22) (2025) 17089–17101, https://doi.org/10.1039/d5ra02399h.

[10] M. Lafitte, R. Dwivedi, R. Elancheliyan, F. Lagugné-Labarthet, L. Buisson, I. Ly, P. Barois, A. Baron, O. Mondain-Monval, V. Ponsinet, Colloidal Self-Assembly of Silver Nanoparticle Clusters for Optical Metasurfaces, Langmuir 40 (5) (2024) 2601–2615, https://doi.org/10.1021/acs.langmuir.3c02900.

[11] A. Panáček, L. Kvítek, R. Prucek, M. Kolář, R. Večeřová, N. Pizúrová, V.K. Sharma, T. Nevěčná, R. Zbořil, Silver Colloid Nanoparticles: Synthesis, Characterization, and their Antibacterial activity, J. Phys. Chem. B 110 (33) (2006) 16248–16253, https://doi.org/10.1021/JP063826H.

[12] D.J. Barillo, D.E. Marx, Silver in Medicine: a Brief history BC 335 to present, Burns 40 (S1) (2014) S3–S8, https://doi.org/10.1016/J.BURNS.2014.09.009.

[13] A. Gauna, Í. Moglia, D. Vásquez, F. Celis, F. Guzmán, F. Sánchez, M. Huerta, C. Álamos, E. Araya, M.J. Kogan, Antimicrobial Coating based on Mussel Adhesive and Silver Nanoparticle-Binding Sequences for Surface Modification of Titanium, Colloids Surf A Physicochem Eng Asp 719 (2025), https://doi.org/10.1016/j.colsurfa.2025.136939.

[14] J. Puttawong, M. Yingkajorn, P. Khongkow, S.D. Thamphiwatana, T. Phairatana, Anti-Methicillin-Resistant Staphylococcus Aureus Efficacy of Layer-by-Layer Silver Nanoparticle/Polyacrylic Acid-Coated Titanium using an In-House dip Coater, Polymers (basel) 17 (3) (2025), https://doi.org/10.3390/polym17030333.

[15] Raju, K. A. K.; Biswas, A. Surface Modifications and Coatings to Improve Osseointegration and Antimicrobial Activity on Titanium Surfaces: A Statistical Review over the Last Decade. *Journal of Orthopaedics*. Reed Elsevier India Pvt. Ltd. September 1, 2025, pp 68–87. doi: 10.1016/j.jor.2025.01.002.

[16] L. Rizzello, P.P. Pompa, Nanosilver-based Antibacterial Drugs and Devices: Mechanisms, Methodological Drawbacks, and guidelines, Chem. Soc. Rev. 43 (5) (2014) 1501–1518, https://doi.org/10.1039/C3CS60218D.

[17] T. Bruna, F. Maldonado-Bravo, P. Jara, N. Caro, Silver Nanoparticles and their Antibacterial applications, Int. J. Mol. Sci. 22 (13) (2021) 7202, https://doi.org/10.3390/ijms22137202.

[18] Z. Xu, C. Zhang, X. Wang, D. Liu, Release strategies of Silver Ions from Materials for Bacterial Killing, ACS Appl. Bio Mater. 4 (5) (2021) 3985–3999, https://doi.org/10.1021/acsabm.0c01485.

[19] C. Carlson, S.M. Hussain, A.M. Schrand, K. Braydich-Stolle, L., Hess, K. L., Jones, R. L., Schlager, J. J., Unique Cellular Interaction of Silver Nanoparticles: Size-Dependent Generation of Reactive Oxygen Species, J. Phys. Chem. B 112 (43) (2008) 13608–13619, https://doi.org/10.1021/jp712087m.

[20] A. Salleh, R. Naomi, N.D. Utami, A.W. Mohammad, E. Mahmoudi, N. Mustafa, M. B. Fauzi, The potential of Silver Nanoparticles for Antiviral and Antibacterial applications: a Mechanism of Action, Nanomaterials (basel) 10 (8) (2020) 1–20, https://doi.org/10.3390/NANO10081566.

[21] L.M. Stabryla, K.A. Johnston, J.E. Millstone, L.M. Gilbertson, Emerging Investigator Series: It's not all about the Ion: support for Particle-specific Contributions to Silver Nanoparticle Antimicrobial activity, Environ. Sci. Nano 5 (9) (2018) 2047–2068, https://doi.org/10.1039/C8EN00429C.

[22] L.A. Tamayo, P.A. Zapata, N.D. Vejar, M.I. Azócar, M.A. Gulppi, X. Zhou, G. E. Thompson, F.M. Rabagliati, M.A. Páez, Release of silver and Copper Nanoparticles from Polyethylene Nanocomposites and their Penetration into Listeria Monocytogenes, Mater. Sci. Eng. C 40 (2014) 24–31, https://doi.org/10.1016/J.MSEC.2014.03.037.

[23] M. Kumari, S. Pandey, V.P. Giri, A. Bhattacharya, R. Shukla, A. Mishra, C. S. Nautiyal, Tailoring Shape and size of Biogenic Silver Nanoparticles to Enhance Antimicrobial Efficacy against MDR Bacteria, Microb. Pathog. 105 (2017) 346–355, https://doi.org/10.1016/J.MICPATH.2016.11.012.

[24] Z. Lu, K. Rong, J. Li, H. Yang, R. Chen, Size-Dependent Antibacterial Activities of Silver Nanoparticles against Oral Anaerobic Pathogenic Bacteria, J. Mater. Sci. Mater. Med. 24 (6) (2013) 1465–1471, https://doi.org/10.1007/s10856-013-4894-5.

[25] J.P. Ruparelia, A.K. Chatterjee, S.P. Duttagupta, S. Mukherji, Strain Specificity in Antimicrobial activity of silver and Copper Nanoparticles, Acta Biomater. 4 (3) (2008) 707–716, https://doi.org/10.1016/J.ACTBIO.2007.11.006.

[26] A. Avalos, A.I. Haza, D. Mateo, P. Morales, Interactions of Manufactured Silver Nanoparticles of Different Sizes with Normal Human Dermal Fibroblasts, Int. Wound J. 13 (1) (2016) 101–109, https://doi.org/10.1111/IWJ.12244.

[27] Chemistry (2021), https://doi.org/10.1039/9781839163623.

[28] Dheyab, M. A.; Aziz, A. A.; Nowfal, S. H.; Braim, F. S.; Abdullah, W.; Kasasbeh, W. H.; Jameel, M. S.; Alanezi, S. T.; Alrosan, M.; Oladzadabbasabadi, N. Sustainable Green Synthesis of Silver Nanoparticles for Safer Biomedical Application. *Journal of Environmental Chemical Engineering*. Elsevier Ltd April 1, 2025. doi: 10.1016/j.jece.2025.115998.

[29] Castañeda-Aude, J. E.; Morones-Ramírez, J. R.; De Haro-Del Río, D. A.; León-Buitimea, A.; Barriga-Castro, E. D.; Escárcega-González, C. E. Ultra-Small Silver Nanoparticles: A Sustainable Green Synthesis Approach for Antibacterial Activity. *Antibiotics 2023, Vol. 12, Page 574* **2023**, *12* (3), 574. doi: 10.3390/ANTIBIOTICS12030574.

[30] J. Roh, H.N. Umh, J. Sim, S. Park, J. Yi, Y. Kim, Dispersion Stability of Citrate- and PVP-AgNPs in Biological Media for Cytotoxicity Test, Korean J. Chem. Eng. 30 (3) (2013) 671–674, https://doi.org/10.1007/S11814-012-0172-3/METRICS.

[31] J.M. Ahn, H.J. Eom, X. Yang, J.N. Meyer, J. Choi, Comparative Toxicity of Silver Nanoparticles on Oxidative stress and DNA damage in the Nematode, Caenorhabditis Elegans. Chemosphere 108 (2014) 343–352, https://doi.org/10.1016/J.CHEMOSPHERE.2014.01.078.

[32] Y. Xia, Y. Xiong, B. Lim, S.E. Skrabalak, Shape-Controlled Synthesis of Metal Nanocrystals: simple Chemistry Meets complex Physics? Angew. Chem. Int. Ed. 48 (1) (2009) 60–103, https://doi.org/10.1002/ANIE.200802248.

[33] S. Ahlberg, A. Antonopulos, J. Diendorf, R. Dringen, M. Epple, R. Flöck, W. Goedecke, C. Graf, N. Haberl, J. Helmlinger, F. Herzog, F. Heuer, S. Hirn, C. Johannes, S. Kittler, M. Köller, K. Korn, W.G. Kreyling, F. Krombach, J. Lademann, K. Loza, E.M. Luther, M. Malissek, M.C. Meinke, D. Nordmeyer, A. Pailliart, J. Raabe, F. Rancan, B. Rothen-Rutishauser, E. Rühl, C. Schleh, A. Seibel, C. Sengstock, L. Treuel, A. Vogt, K. Weber, R.Z. Review, PVP-Coated, Negatively Charged Silver Nanoparticles: a Multi-Center Study of their Physicochemical Characteristics, Cell Culture and in Vivo Experiments, Beilstein J. Nanotechnol. 5 (2014) 1944–1965, https://doi.org/10.3762/bjnano.5.205.

[34] K. Ishizu, H. Kakinuma, K. Ochi, S. Uchida, M. Hayashi, Encapsulation of Silver Nanoparticles within Double-Cylinder-Type Copolymer Brushes as Templates, Polym. Adv. Technol. 16 (11–12) (2005) 834–839, https://doi.org/10.1002/PAT.660.

[35] S. Sugihara, M. Sudo, Y. Maeda, Synthesis and Nano-Object Assembly of Biomimetic Block Copolymers for Catalytic Silver Nanoparticles, Langmuir 35 (5) (2019) 1346–1356, https://doi.org/10.1021/acs.langmuir.8b01558.

[36] B. Yuan, J. Guo, S. Bai, In Situ Thermally Induced Reduction of Silver Nitrate by polyvinyl Alcohol to Prepare a Three-Dimensional Porous Ag Substrate with Excellent Adsorption and Surface-Enhanced Raman Scattering Properties †, J. Mater. Chem. C 8 (2020) 6478, https://doi.org/10.1039/d0tc00772b.

[37] S.S. Soni, R.L. Vekariya, V.K. Aswal, Ionic Liquid Induced Sphere-to-Ribbon transition in the Block Copolymer Mediated Synthesis of Silver Nanoparticles, RSC Adv. 3 (22) (2013) 8398–8406, https://doi.org/10.1039/C3RA41138A.

[38] P.D. Petrov, K. Yoncheva, V. Gancheva, S. Konstantinov, B. Trzebicka, Multifunctional Block Copolymer Nanocarriers for Co-delivery of Silver Nanoparticles and Curcumin: Synthesis and Enhanced Efficacy against Tumor Cells, Eur. Polym. J. 81 (2016) 24–33, https://doi.org/10.1016/J.EURPOLYMJ.2016.05.010.

[39] A.A. Zharikov, E.A. Zezina, A.V. Sybachin, A.L. Vasiliev, Emel'yanov, A. I., Pozdnyakov, A. S., Feldman, V. I., Zezin, A. A., Effect of "Corona-Core" Structuring of Poly(1-Vinyl-1,2,4-Triazole)–Poly(Acrylic Acid)-Ag(I) Interpolymer Complexes on the Radiation-Induced Preparation and Stability of Silver Nanoparticles, Radiat. Phys. Chem. 224 (2024) 112059, https://doi.org/10.1016/J.RADPHYSCHEM.2024.112059.

[40] Y. Zhang, H. Peng, W. Huang, Y. Zhou, X. Zhang, D. Yan, Hyperbranched Poly (Amidoamine) as the Stabilizer and Reductant to Prepare Colloid Silver Nanoparticles in Situ and their Antibacterial activity, J. Phys. Chem. C 112 (7) (2008) 2330–2336, https://doi.org/10.1021/jp075436g.

[41] A. Frattini, N. Pellegri, D. Nicastro, O. De Sanctis, Effect of Amine groups in the Synthesis of Ag Nanoparticles using Aminosilanes, Mater. Chem. Phys. 94 (1) (2005) 148–152, https://doi.org/10.1016/J.MATCHEMPHYS.2005.04.023.

[42] A.M. Yon, B.J.D. Marty, C.D. Ciuculescu-Pradines, Amines and Amine-Boranes. In *RSC Nanoscience and Nanotechnology*; Royal Society of, Chemistry Vol. 2021-January (2021) 130–156, https://doi.org/10.1039/9781839163623-00130.

[43] J.D.S. Newman, G.J. Blanchard, Formation of Gold Nanoparticles using Amine reducing Agents, Langmuir 22 (13) (2006) 5882–5887, https://doi.org/10.1021/LA060045Z/SUPPL_FILE/LA060045ZSI20060401_065759.PDF.

[44] P.J. Smith, C.K. Mann, Electrochemical Dealkylation of Aliphatic Amines, J. Org. Chem. 34 (6) (1969) 1821–1826, https://doi.org/10.1021/JO01258A063/ASSET/JO01258A063.FP.PNG_V03.

[45] A. Adenier, M.M. Chehimi, I. Gallardo, J. Pinson, N. Vilà, Electrochemical Oxidation of Aliphatic Amines and their Attachment to Carbon and Metal Surfaces, Langmuir 20 (19) (2004) 8243–8253, https://doi.org/10.1021/LA049194C/SUPPL_FILE/LA049194CSI20040701_042438.PDF.

[46] C. Subramaniam, R.T. Tom, T. Pradeep, On the Formation of Protected Gold Nanoparticles from AuCl 4- by the Reduction using Aromatic Amines, J. Nanopart. Res. 7 (2–3) (2005) 209–217, https://doi.org/10.1007/S11051-005-0315-0/METRICS.

[47] de Montellano, P. R. O. Cytochrome P450: Structure, Mechanism, and Biochemistry, Fourth Edition. *Cytochrome P450: Structure, Mechanism, and Biochemistry, Fourth Edition* **2015**, 1–905. doi: 10.1007/978-3-319-12108-6/COVER.

[48] E. Baciocchi, M. Bietti, O. Lanzalunga, A. Lapi, D. Raponi, N-Demethylation of N,N-Dimethylanilines by the Benzotriazole N-Oxyl Radical: evidence for a Two-step Electron Transfer-Proton transfer Mechanism, J. Org. Chem. 75 (5) (2010) 1378–1385, https://doi.org/10.1021/JO100040Y/SUPPL_FILE/JO100040Y_SI_001.PDF.

[49] D.M. Mazur, A.S. Surmillo, S.A. Sypalov, I.S. Varsegov, Ul'yanovskii, N. V., Kosyakov, D. S., Lebedev, A. T., N-Dealkylation of Amines during Water Disinfection – Revealing a New direction in the Formation of Disinfection by-Products, Chemosphere 350 (2024) 141117, https://doi.org/10.1016/J.CHEMOSPHERE.2024.141117.

[50] M. He, Q. Wang, R. Wang, Y. Xie, W. Zhao, C. Zhao, Design of Antibacterial Poly (Ether Sulfone) Membranes via Covalently Attaching Hydrogel Thin Layers Loaded with Ag Nanoparticles, ACS Appl. Mater. Interfaces 9 (19) (2017) 15962–15974, https://doi.org/10.1021/ACSAMI.7B03176/SUPPL_FILE/AM7B03176_SI_001.PDF.

[51] N. Kutsevol, V. Chumachenko, V. Shkodich, N. Temnikova, M. Rawiso, V. Solntsev, Green Route Synthesis of Nanosilver into Polyelectrolyte Solutions at High PH Value, Mol. Cryst. Liq. Cryst. 640 (1) (2016) 90–97, https://doi.org/10.1080/15421406.2016.1255519.

[52] H. Li, R. Luo, J. Qu, Poly(Methyl Methacrylate-Co-Butyl Acrylate) Copolymer/Ag Nanocomposites Prepared by Latex Mixing for Multifunctional Coatings, Polym. Compos. 45 (3) (2024) 2795–2808, https://doi.org/10.1002/PC.27958.

[53] Y.M. Mohan, T. Premkumar, K. Lee, K.E. Geckeler, Fabrication of Silver Nanoparticles in Hydrogel Networks, Macromol. Rapid Commun. 27 (16) (2006) 1346–1354, https://doi.org/10.1002/MARC.200600297.

[54] P. Bhol, M. Mohanty, P.S. Mohanty, Polymer-Matrix Stabilized Metal Nanoparticles: Synthesis, Characterizations and Insight into Molecular Interactions between Metal Ions, Atoms and Polymer Moieties, J. Mol. Liq. 325 (2021) 115135, https://doi.org/10.1016/J.MOLLIQ.2020.115135.

[55] Yamada, T.; Fukuhara, K.; Matsuoka, K.; Minemawari, H.; Tsutsumi, J.; Fukuda, N.; Aoshima, K.; Arai, S.; Makita, Y.; Kubo, H.; Enomoto, T.; Togashi, T.; Kurihara, M.; Hasegawa, T. Nanoparticle Chemisorption Printing Technique for Conductive Silver Patterning with Submicron Resolution. *Nature Communications 2016 7:1* **2016**, *7* (1), 1–9. doi: 10.1038/ncomms11402.

[56] P. Gentili, M. Nardi, I. Antignano, P. Cambise, M. D'Abramo, F. D'Acunzo, A. Pinna, E. Ussia, 2-(Hydroxyimino)Aldehydes: Photo- and Physicochemical Properties of a Versatile Functional Group for Monomer Design, Chem. A Eur. J. 24 (30) (2018) 7683–7694, https://doi.org/10.1002/chem.201800059.

[57] I. Antignano, et al., Influence of Nanoaggregation Routes on the Structure and thermal Behavior of Multiple-Stimuli Responsive Micelles from Block Copolymers of OEGMA and the Weak Acid [2-(Hydroxyimino)Aldehyde]Butyl Methacrylate, Langmuir (2022).

[58] I. Antignano, S. Casciardi, F. D'Acunzo, A. Del Giudice, L. Gatti, P. Gentili, F. Mura, A. Ricci, G. Masci, Hybrid Copper-Polyelectrolyte Nanoaggregates Obtained with

Smart Block Copolymers based on 4-[(Hydroxyimino)Aldehyde]Butyl Methacrylate (HIABMA) in Water and Acetonitrile, Polymer (guildf) 306 (2024) 127197, https://doi.org/10.1016/j.polymer.2024.127197.
[59] N. Yuan, T. Su, L. Zhang, D. Li, J. Li, T. Zhu, J. Hu, H. Guo, Y. Liu, N. Liu, W. Han, D. Yao, A Novel Approach for Synthesizing Ultra–Small Silver Nanoparticles using Covalent Organic Frameworks as Template, Stabilizer and Reductant at Room Temperature, ChemistrySelect 9 (16) (2024) e202304718, https://doi.org/10.1002/SLCT.202304718.
[60] K. Sakai-Kato, N. Nishiyama, M. Kozaki, T. Nakanishi, Y. Matsuda, M. Hirano, H. Hanada, S. Hisada, H. Onodera, H. Harashima, Y. Matsumura, K. Kataoka, Y. Goda, H. Okuda, T. Kawanishi, General Considerations Regarding the in Vitro and in Vivo Properties of Block Copolymer Micelle Products and their Evaluation, J. Control. Release 210 (2015) 76–83, https://doi.org/10.1016/J.JCONREL.2015.05.259.
[61] M. Sztucki, T. Narayanan, Development of an Ultra-Small-Angle X-Ray Scattering Instrument for probing the Microstructure and the Dynamics of Soft Matter, J. Appl. Crystallogr. 40 (s1) (2006) s459–s462, https://doi.org/10.1107/S0021889806045833.
[62] K. Manalastas-Cantos, P.V. Konarev, N.R. Hajizadeh, A.G. Kikhney, M. V. Petoukhov, D.S. Molodenskiy, A. Panjkovich, H.D.T. Mertens, A. Gruzinov, C. Borges, C.M. Jeffries, D.I. Svergun, D. Franke, ATSAS 3.0: Expanded Functionality and New Tools for Small-Angle Scattering Data Analysis, J. Appl. Crystallogr. 54 (1) (2021) 343–355, https://doi.org/10.1107/S1600576720013412.
[63] I. Breßler, J. Kohlbrecher, A.F. Thünemann, *SASfit* : a Tool for Small-Angle Scattering Data Analysis using a Library of Analytical Expressions, J. Appl. Crystallogr. 48 (5) (2015) 1587–1598, https://doi.org/10.1107/S1600576715016544.
[64] M. Nardi, F. D'Acunzo, M. Clemente, G. Proietti, P. Gentili, A first Study on Copolymers of a Methacrylate Containing the 2-(Hydroxyimino)Aldehyde Group and OEGMA. RAFT Polymerization and Assessment of thermal and Photoresponsive Polymer Behavior, Polym. Chem. 8 (29) (2017) 4233–4245, https://doi.org/10.1039/c7py00975e.
[65] O.A.D. Gallardo, R. Moiraghi, M.A. Macchione, J.A. Godoy, M.A. Pérez, E. A. Coronado, V.A. Macagno, Silver Oxide Particles/Silver Nanoparticles Interconversion: Susceptibility of Forward/Backward Reactions to the Chemical Environment at Room Temperature, RSC Adv. 2 (7) (2012) 2923, https://doi.org/10.1039/c2ra01044e.
[66] M.A. Ogliaruso, J.F. Wolfe, The Synthesis of Carboxylic Acids and Esters and their Derivatives, Supplement b: the Chemistry of Acid Derivatives: Part 1 (1) (2010) 267–490, https://doi.org/10.1002/9780470771587.CH7.
[67] J.F. Gomes, A.C. Garcia, E.B. Ferreira, C. Pires, V.L. Oliveira, G. Tremiliosi-Filho, L. H.S. Gasparotto, New Insights into the Formation Mechanism of Ag, Au and AgAu Nanoparticles in Aqueous Alkaline Media: Alkoxides from Alcohols, Aldehydes and Ketones as Universal reducing Agents, PCCP 17 (33) (2015) 21683–21693, https://doi.org/10.1039/c5cp02155c.
[68] A.W. Apblett, G.D. Georgieva, J.T. Mague, Spectroscopic and Thermochemical Investigation of Alkaline Earth Metal Salts of 2-Oximinopropionate, Can. J. Chem. 75 (5) (1997) 483–490, https://doi.org/10.1139/V97-056.
[69] S. Tadjiki, M.D. Montaño, S. Assemi, A. Barber, J. Ranville, R. Beckett, Measurement of the Density of Engineered Silver Nanoparticles using Centrifugal FFF-TEM and Single Particle ICP-MS, Anal. Chem. 89 (11) (2017) 6056–6064, https://doi.org/10.1021/ACS.ANALCHEM.7B00652/SUPPL_FILE/AC7B00652_SI_001.PDF.
[70] M. Keerl, J.S. Pedersen, W. Richtering, Temperature Sensitive Copolymer Microgels with Nanophase Separated Structure, J. Am. Chem. Soc. 131 (8) (2009) 3093–3097, https://doi.org/10.1021/JA807367P/ASSET/IMAGES/MEDIUM/JA-2008-07367P_0004.GIF.
[71] B.H. Elwakil A.M. Eldrieny A. Rashed Z. Almotairy M. El-Khatib Potent Biological activity of newly Fabricated Silver Nanoparticles Coated by a Carbon Shell Synthesized by Electrical Arc Scientific Reports | 14 123AD, 5324 10.1038/s41598-024-54648-y.
[72] V. Balamurugan, C. Ragavendran, D. Arulbalachandran, A. Fahad Alrefaei, R. Rajendran, Green Synthesis of Silver Nanoparticles using Pandanus Tectorius Aerial root Extract: Characterization, Antibacterial, Cytotoxic, and Photocatalytic Properties, and Ecotoxicological Assessment, Inorg. Chem. Commun. 168 (2024) 112882, https://doi.org/10.1016/J.INOCHE.2024.112882.
[73] Ghasemi, S.; Dabirian, S.; Kariminejad, F.; Koohi, D. E.; Nemattalab, M.; Majidimoghadam, S.; Zamani, E.; Yousefbeyk, F. Process Optimization for Green Synthesis of Silver Nanoparticles Using Rubus Discolor Leaves Extract and Its Biological Activities against Multi-Drug Resistant Bacteria and Cancer Cells. *Scientific Reports 2024 14:1* **2024**, *14* (1), 1–19. doi: 10.1038/s41598-024-54702-9.
[74] Castañeda-Aude, J. E.; Morones-Ramírez, J. R.; De Haro-Del Río, D. A.; León-Buitimea, A.; Barriga-Castro, E. D.; Escárcega-González, C. E. Ultra-Small Silver Nanoparticles: A Sustainable Green Synthesis Approach for Antibacterial Activity. *Antibiotics 2023, Vol. 12, Page 574* **2023**, *12* (3), 574. doi: 10.3390/ANTIBIOTICS12030574.
[75] V. Badineni, H. Maseed, S.K. Arla, S. Yerramala, V.K. Naidu, B., Kaviyarasu, K., Effect of PVA/PVP protective Agent on the Formation of Silver Nanoparticles and its Photocatalytic and Antimicrobial activity, In Materials Today: Proceedings; Elsevier Ltd 36 (2019) 121–125, https://doi.org/10.1016/j.matpr.2020.02.002.
[76] J. Liu, X. Li, L. Liu, Q. Bai, N. Sui, Z. Zhu, Self-Assembled Ultrasmall Silver Nanoclusters on Liposome for Topical Antimicrobial delivery, Colloids Surf. B Biointerfaces 200 (2021) 111618, https://doi.org/10.1016/J.COLSURFB.2021.111618.
[77] H.M. Abdelmigid, M.M. Morsi, N.A. Hussien, A.A. Alyamani, N.M. Al Sufyani, Comparative Analysis of Nanosilver Particles Synthesized by Different Approaches and their Antimicrobial Efficacy, J. Nanomater. 2021 (1) (2021) 2204776, https://doi.org/10.1155/2021/2204776.
[78] T. Ameh, K. Zarzosa, J. Dickinson, W.E. Braswell, C.M. Sayes, Nanoparticle Surface stabilizing Agents Influence Antibacterial Action, Front. Microbiol. 14 (2023) 1119550, https://doi.org/10.3389/FMICB.2023.1119550/BIBTEX.
[79] Franci, G.; Falanga, A.; Galdiero, S.; Palomba, L.; Rai, M.; Morelli, G.; Galdiero, M. Silver Nanoparticles as Potential Antibacterial Agents. *Molecules 2015, Vol. 20, Pages 8856-8874* **2015**, *20* (5), 8856–8874. doi: 10.3390/MOLECULES20058856.
[80] M. Mahmood, M. Abid, M.F. Nazar, M.N. Zafar, M.A. Raza, M. Ashfaq, A.M. Khan, S.H. Sumrra, M. Zubair, The Wet Chemical Synthesis of Surfactant-Capped Quasi-Spherical Silver Nanoparticles with Enhanced Antibacterial activity, Mater. Adv. 1 (7) (2020) 2332–2338, https://doi.org/10.1039/D0MA00408A.
[81] S. Arokiyaraj, S. Vincent, M. Saravanan, Y. Lee, Y.K. Oh, K.H. Kim, Green Synthesis of Silver Nanoparticles using Rheum Palmatum root Extract and their Antibacterial activity against Staphylococcus Aureus and Pseudomonas Aeruginosa, Artif. Cells Nanomed. Biotechnol. 45 (2) (2017) 372–379, https://doi.org/10.3109/21691401.2016.1160403.
[82] R. Salomoni, P. Léo, A.F. Montemor, B.G. Rinaldi, M.F.A. Rodrigues, Antibacterial effect of Silver Nanoparticles in Pseudomonas Aeruginosa, Nanotechnol. Sci. Appl. 10 (2017) 115–121, https://doi.org/10.2147/NSA.S133415.
[83] K. Rezapour, M. Mousavizadegan, S.M.R. Mortazavi, M. Golbashy, M. Hosseini, Enhanced Antibacterial effect of Kanamycin-Stabilized Nanoclusters, ChemistrySelect 9 (48) (2024) e202403849, https://doi.org/10.1002/SLCT.202403849.